AGU PUBLICATIONS

JGR

Journal of Geophysical Research: Planets

RESEARCH ARTICLE
10.1002/2016JE005111

This article is a companion to *Smith et al.* [2017] doi:10.1002/2016JE005112.

Key Points:
- Acid alteration at moderate pH produces mineral precipitates but has little to no physical or spectral effect on the underlying basalt
- Acid alteration at low pH causes significant leaching, but altered basalt and glass exhibit different near-infrared and thermal infrared spectra
- The spectral difference is due to different weathering mechanisms and may allow us to uniquely detect leached glasses on Mars

Correspondence to:
B. H. N. Horgan,
briony@purdue.edu

Citation:
Horgan, B. H. N., R. J. Smith, E. A. Cloutis, P. Mann, and P. R. Christensen (2017), Acidic weathering of basalt and basaltic glass: 1. Near-infrared spectra, thermal infrared spectra, and implications for Mars, *J. Geophys. Res. Planets*, *122*, 172–202, doi:10.1002/2016JE005111.

Received 17 JUN 2016
Accepted 15 SEP 2016
Accepted article online 3 JAN 2017
Published online 24 JAN 2017

Acidic weathering of basalt and basaltic glass: 1. Near-infrared spectra, thermal infrared spectra, and implications for Mars

Briony H. N. Horgan[1], Rebecca J. Smith[1,2], Edward A. Cloutis[3], Paul Mann[3], and Philip R. Christensen[2]

[1]Department of Earth, Atmospheric, and Planetary Sciences, Purdue University, West Lafayette, Indiana, USA, [2]School of Earth and Space Exploration, Arizona State University, Tempe, Arizona, USA, [3]Department of Geography, University of Winnipeg, Winnipeg, Manitoba, Canada

Abstract Acid-leached rinds and coatings occur in volcanic environments on Earth and have been identified using orbital spectroscopy on Mars, but their development is poorly understood. We simulated long-term open-system acidic weathering in a laboratory by repeatedly rinsing and submerging crystalline and glassy basalts in pH ~ 1 and pH ~ 3 acidic solutions for 213 days and compared their visible/near-infrared (0.3–2.5 μm) and thermal infrared (5–50 μm) spectral characteristics to their microscopic physical and chemical properties from scanning electron microscopy (SEM). We find that while alteration at moderately low pH (~3) can produce mineral precipitates from solution, it has very little spectral or physical effect on the underlying parent material. In contrast, alteration at very low pH (~1) results in clear silica spectral signatures for all crystalline samples while glasses exhibit strong blue concave-up near-infrared slopes. SEM indicates that these spectral differences correspond to different modes of alteration. In glass, alteration occurs only at the surface and produces a silica-enriched leached rind, while in more crystalline samples, alteration penetrates the interior to cause dissolution and replacement by silica. We confirm that glass is more stable than crystalline basalt under long-term acidic leaching, suggesting that glass could be enriched and common in terrains on Mars that have been exposed to acidic weathering. Leached glasses are consistent with both OMEGA and Thermal Emission Spectrometer (TES) spectra of the Martian northern lowlands and may contribute to the high-silica phases detected globally in TES Surface Type 2. Thus, both glass-rich deposits and acidic weathering may have been widespread on Mars.

1. Introduction

Acidic weathering creates a unique suite of alteration products that are not observed under the neutral to alkaline weathering conditions that are more common in aqueous environments on Earth. On Mars, the products of acidic alteration appear to be widespread and have been used to support the hypothesis that the Martian environment became much more acidic and oxidizing through time [e.g., *Bibring et al.*, 2006]. In addition to the acid sulfates observed at sites like Meridiani Planum and Mawrth Vallis [*Squyres et al.*, 2004; *Farrand et al.*, 2009], recent studies have shown that the low-albedo regions of the North Polar Sand Sea and much of the northern plains of Mars are spectrally consistent with acid-leached glass [*Horgan and Bell*, 2012]. This inference of leached glass is based on studies of the near-infrared spectra of volcanic glasses altered naturally in situ by acidic fluids at low water:rock ratios, which produce very thin leached and silica-enriched rinds on the surface of glass, often overlain by silica-rich coatings [*Minitti et al.*, 2007; *Seelos et al.*, 2010; *Chemtob et al.*, 2010]. However, the origin of the unique near-infrared spectral signature of the rinds and their spectral development over time are poorly understood.

One method that could confirm the presence of acid-leached glass at these locations on Mars would be thermal infrared spectra from instruments like the Thermal Emission Spectrometer (TES) [*Christensen et al.*, 2001]. Intriguingly, the regions on Mars where near-infrared spectra are consistent with leached glass coincide with regions that are also spectrally distinct in TES thermal infrared spectra. Unlike the more common olivine basalt composition (TES Surface Type 1), models of spectra from the northern plains and several other locations on Mars require an additional high-silica component (TES Surface Type 2) [*Bandfield et al.*, 2000]. The nature of this high-silica component is not well constrained and could be consistent either with primary volcanic glasses (e.g., obsidian in an andesitic basalt) [*Bandfield et al.*, 2000] or with secondary alteration products (e.g., opal, zeolites, allophane, and silica coatings) [*Kraft et al.*, 2003;

Wyatt and McSween et al., 2002; *Michalski et al*., 2005; *Ruff and Christensen*, 2007; *Rampe et al*., 2012]. The close association between the near-infrared signatures of leached glass and TES high-silica phases in the northern plains suggests that silica rinds could be the dominant high-silica phase in TES Surface Type 2. However, the effect of leached rinds on the thermal infrared spectra of glasses and whether or not this could be spectrally consistent with TES Surface Type 2 are not well understood. Previous studies of natural leached glasses indicated a possible consistency with TES Surface Type 2 [*Minitti et al*., 2007], but their thermal infrared spectra have not been investigated in detail.

Thus, in this study, we seek to understand the near-infrared and thermal infrared spectral effects of acidic weathering on basaltic glasses, how those spectral effects differ from those caused by acidic weathering of crystalline basalts, and how varying pH affects basaltic weathering. This basic understanding may help us to constrain the composition and weathering history of large regions of the Martian surface.

2. Background

2.1. Previous Acidic Weathering Experiments

Previous experiments have simulated acidic weathering of basalts on Mars, with a focus on the secondary minerals produced by these processes. In general, these studies have found that highly acidic alteration (starting pH 0–1) leads to precipitation of sulfates and silica, while more moderately acidic alteration (starting pH 3–4) mainly leads to precipitation of iron oxides. However, an important additional outcome of many of these experiments is that glasses behave differently and are often less reactive under acidic alteration than their crystalline counterparts.

Banin et al. [1997] submerged palagonitized basaltic tephra in acidic fluids at a water:rock ratio of 1 for 7 days at 25°C (a closed system) and showed that gypsum and alunogen were the primary alteration products using X-ray diffraction. In a similar closed system experiment, *Tosca et al*. [2004] submerged sand-sized basaltic andesite (~57 wt % SiO_2), basalt (~48 wt % SiO_2), and their glass counterparts in acidic fluids of varying concentrations (starting pH 0–4) at a water:rock ratio of 10. The results after 14 days at 25°C varied with both crystallinity and composition. For the crystalline samples, highly acidic weathering favored deposition of sulfates and amorphous silica while the solution maintained a persistently acidic pH, and moderately acidic weathering released enough solutes to buffer the solution to higher pH and then precipitated iron oxides. At low pH, precipitation of amorphous silica and Fe/Mg sulfates was enhanced by the dissolution of olivine in the basalt, while Ca sulfate precipitation was related to dissolution of Ca-bearing pyroxene and plagioclase feldspar in both the basalt and basaltic andesites. Follow-up experiments by *Yant et al*. [2016] recreated the *Tosca et al*. [2004] experiments over a period of 14 days with an expanded suite of glasses and showed that more mafic glasses showed more intense alteration spectral signatures than the more silicic glasses over the duration of the experiment, including strong silica and sulfate signatures and blue spectral slopes in the visible/near-infrared and silica absorptions in the thermal infrared.

The glass samples in *Tosca et al*. [2004] behaved quite differently from their crystalline counterparts. The high-Si (basaltic andesite) glass dissolved nonstoichiometrically, indicating that the glassy SiO_4 network was more resilient to dissolution than network-modifying cations (Fe^{2+}, Mg^{2+}, Ca^{2+}, Na^{+}, etc.). This effect was more pronounced at higher pH (starting pH 4, buffered up to 11), which caused significant removal of Na^{+} and deposition of halite (NaCl). At lower pH (starting pH 1–2, buffered up to 6), the high-Si glass was actually more resistant to dissolution than either of the crystalline samples, producing only poorly crystalline Na/Ca sulfates and minor gypsum from removal of Ca. At low pH (starting pH 0, buffered to 1), the high-Si glass initially dissolved stoichiometrically to form amorphous silica coatings but rapidly ceased dissolution altogether once the coatings became thick enough to prevent further infiltration. In contrast, the low-Si (basaltic) glass completely dissolved to form amorphous silica at very low pH and formed coatings of iron oxides at higher pH. These results are consistent with the observation that the dissolution rate of glasses in both natural and laboratory environments is inversely proportional to silica content [*Glass*, 1984; *Wolff-Boenisch et al*., 2004].

In order to test the effects of different alteration conditions on alteration precipitates, *Golden et al*. [2005] performed similar closed system experiments at water:rock ratios of >100 alongside open-system (three-

stage) and vapor alteration experiments, all 6 days in total length, at high temperature (145°C), and a very low starting pH (0–1). The materials in these experiments included an olivine-rich basaltic sand and a plagioclase and glass-rich basaltic tephra, as loose 500–1000 μm grains, ground and sieved to <53 μm loose grains, and as compressed thick sections. In the closed system experiments, they found that amorphous silica was the primary precipitate for all samples, similar to the very low pH *Tosca et al*. [2004] results. The open-system and acid fog (vapor alteration) experiments gave similar results, with additional precipitation of Mg/Fe/Al sulfates in all olivine-bearing samples and additional Ca sulfates in all samples in the acid fog experiments. Although the effects on primary phases were not a focus of this study, the authors did note that basaltic glass appeared to be the least reactive phase under acidic leaching in all experiments, followed by plagioclase and then olivine as the most reactive. Subsequent modeling has suggested that pyroxene falls between olivine and plagioclase on this scale [*McAdam et al*., 2008].

In a further permutation of possible weathering regimes, *Hurowitz et al*. [2005] conducted flow-through acidic weathering experiments on basalts, using both entirely fresh fluids and multiple batches of recycled fluids at water:rock ratios of 100 and 1000, for up to 17 days. Evaporite minerals from these experiments were dominated by sulfates and amorphous silica, similar to previous experiments, with significantly more sulfates produced under batch experiments. SEM and Raman analyses of reacted basalt indicated significant amorphous silica as well as limited occurrences of poorly crystalline iron oxide phases, potentially consistent with ferrihydrite.

Marcucci and Hynek [2014] exposed plagioclase, olivine, and pyroxene mineral separates and basaltic cinders to acidic alteration (starting pH 0–3.5) under closed system, hydrothermal conditions (65°C, 150°C, and 200°C) with variable water:rock ratios between 1 and 10 for up to 60 days. The main alteration products in their experiments included diverse sulfates with compositions corresponding to cations that were available from the primary phase undergoing weathering. They found that varying the experimental conditions within the parameter ranges of their experiments did not significantly affect the mineralogy of precipitated alteration products but did alter their relative abundance. Plagioclase and olivine weathering both produced significant amorphous silica coatings, with aluminum-bearing silica coatings forming on plagioclase. While all of these experiments were conducted at moderate to high temperatures, other dissolution experiments suggest that similar weathering trends persist at low temperature, although the rate of dissolution (especially of silica) is much lower [*Hausrath and Brantley*, 2010].

Together, these results confirm that amorphous silica, sulfates, and sometimes iron oxides are all common secondary minerals produced during acidic weathering of both basalts and basaltic glasses. However, the differences observed in the secondary precipitates and in the relative stability of the crystalline basalts versus the glasses suggest that different mechanisms facilitate acidic weathering in these two phases.

2.2. Acid Leaching of Mineral and Glass Surfaces

In our experiments, we are interested in the effects of acid leaching on primary minerals and glasses, and, in particular, on the formation of leached rinds and precipitated coatings. Previous studies have suggested that these two types of weathering products are formed via different processes [e.g., *Minitti et al*., 2007]. During exposure to acidic fluids, most silicate minerals undergo stoichiometric dissolution, wherein all elements in the silicate structure are extracted at similar rates [e.g., *Ruiz-Agudo et al*., 2012]. Once the elements are in solution, their relative solubilities determine their fate. Oxidized iron and silica both have low solubilities at low to neutral pH and so are often rapidly redeposited on the surface of the mineral as a poorly crystalline or amorphous coating [*Petit et al*., 1990; *King et al*., 2011]. Similar silica-rich and sometimes iron-bearing coatings can form without any alteration of the substrate, such as those due to dissolution of windblown dust in a desert environment or precipitation of transported silica sourced from alteration elsewhere in the system, as in silica sinters or diagenesis of quartz-rich sandstones [*Dorn*, 1998]. Because they have an external source for the silica, these coatings can become very thick, often exceeding millimeters in thickness [*Oguchi*, 2004].

Leached rinds, however, are thought to be unique to glasses and a few other minerals, including some varieties of feldspar. When these phases are exposed to acidic fluids, their dissolution is nonstoichiometric. In the case of glasses, the canonical model is that the polymerized silicate structure and constituent cations (Si^{4+}, Al^{3+}, and Fe^{3+}) in glass are more difficult to remove than the more weakly bound univalent

and divalent network-modifying cations (Fe^{2+}, Mg^{2+}, Ca^{2+}, Na^{+}, etc.), so the network-modifying cations are preferentially removed [*White*, 1983; *Oelkers and Gislason*, 2001]. This produces a residual leached outer rind on the glass surface that is composed exclusively of the silicate network. Thus, this rind appears to be enriched in silica relative to the interior but is actually just depleted in all other major oxides [*Chemtob et al*., 2010]. Alternatively, more recent studies of this process in crystalline minerals have suggested that these apparently leached layers may instead be formed through a highly localized process of total dissolution followed by nonstoichiometric precipitation [*Ruiz-Agudo et al*., 2012; *Hellmann et al*., 2012]. This process may also be responsible for producing leached layers in glasses [*Crovisier et al*., 1987; *Geisler et al*., 2010, 2015]. See our companion paper for a more in-depth discussion of this topic [*Smith et al*., 2017]. For continuity with previous Mars-relevant work [e.g., *Minitti et al*., 2007; *Chemtob et al*., 2010; *Horgan and Bell*, 2012], here we will continue to refer to these leaching and/or dissolution fronts on glass as leached rinds.

In either case, due to their limiting effect on the diffusion rate of additional cations from their substrate, these leached rinds are often self-limiting in their depth and rarely exceed 10 μm [*White*, 1983; *Minitti et al*., 2007; *Chemtob et al*., 2010]. This steady state condition (full rind development) can occur quickly with continuous exposure to low pH. For example, in silicic glass (64–79 wt % SiO_2) dissolution experiments, *White* [1983] found that rinds, as indicated by steady state concentrations of cations in solution, were fully developed after 3 weeks at 25°C and pH 1.0 but were not developed after 6 months at pH 6.2. After their initial exposure and rapid dissolution, leached glasses are highly resistant to further leaching, as dissolution of the rind itself occurs at a much slower rate than the initial cation leaching. Dissolution of the rind occurs as H^{+} from the solution exchanges with Al substituted for Si in the silicate structure, which partially liberates adjoining silica tetrahedral, that eventually becomes detached and dissolves [*Oelkers and Gislason*, 2001]. Deposition of silica coatings on the exterior of the glass can also lead to even slower dissolution of the rind [*Berger et al*., 1994], especially at low pH or at low temperatures where silica solubility is low [*Gislason and Oelkers*, 2003]. Because of this stability under long-term leaching, glass is the most common material used to construct vessels for the underground storage of radioactive materials [*Techer et al*., 2001; *Grambow*, 2006].

2.3. Spectral Signatures of Leached Rinds and Coatings

Leached rinds and silica coatings exhibit different spectral signatures in the near infrared. When hydrated, silica exhibits diagnostic absorption bands near 1.4 and 1.9 μm due to overtones of OH stretching vibrational modes in adsorbed H_2O, as well as a broad doublet absorption band near 2.21 and 2.26 μm due to Si–OH rotation and stretching vibrational modes [e.g., *Langer and Florke*, 1974; *Rice et al*., 2013]. Thick silica coatings on basalt exhibit these absorption bands but also often exhibit a strong blue spectral slope (less reflectance at longer wavelengths) from the visible into the near infrared [*Milliken et al*., 2008]. Similar blue spectral slopes have been observed in studies of other bright coatings, like ferric oxides [*Fischer and Pieters*, 1993]. The skin depth of reflected light is usually estimated to be on the order of the wavelength of the light, so in that study, the cause of the blue slope was hypothesized to be greater skin depths of the reflecting light at longer wavelengths, leading to more absorption by the underlying dark materials and thus decreasing reflectance with increasing wavelengths. In contrast, very thin silica coatings (a few μm thick) do not exhibit either the blue spectral slope or detectable absorption bands [*Kraft et al*., 2007].

Minitti et al. [2007] examined the near-infrared spectra of natural silica-coated glassy basalts from the surface of a 40 year old flow on Mauna Kea, Hawaii. Both the silica absorption bands and the blue spectral slope are present in the spectra of some of the samples. However, other samples exhibit not just blue but also concave-up spectral slopes, the strongest of which occur without corresponding silica absorption bands (leached glass spectra in Figure 2). In a detailed investigation of the samples, *Minitti et al*. [2007] showed that concave-up spectral slopes were exhibited both by some of the white or orange silica coatings and by thin (<3 μm), dull, and dark rinds that appeared to underlie these coatings. *Minitti et al*. [2007] hypothesized that these rinds formed due to acidic leaching, and scanning electron microscope (SEM) and back-scattered electron (BSE) images of these samples confirm that they exhibit residual and silica-enriched glassy rinds consistent with a leaching origin [*Chemtob et al*., 2010]. Based on laboratory and field observations, the leaching most likely occurred due to both syndepositional and postdepositional alteration by acidic volcanic vapors [*Chemtob et al*., 2010]. *Seelos et al*. [2010] confirmed that the leached rind signature is apparent in aerial near-infrared

Table 1. Sample Information

Sample	Description	Surface Type		
		Grains	Cut	Natural
BSB101	Basaltic glass, black sand beach, Hawaii (collected by R.B. Singer)	A, B[a]		
ICE170	Basalt, pillow lava, Dagmalafell, Iceland (collected by E. Cloutis)	A, B	A, B	A, B
BAS101	Basaltic glass, Kilauea Caldera, 1956 flow, Hawaii (collected by E. Cloutis)	A, B	A	A
BAS205	Basalt, Roza dike, Columbia River Plateau (collected by S. Atkinson[b])	A, B	A, B	A, B

[a]A and B indicate which acid solutions were used to weather samples, as described in the text.
[b]*Atkinson* [1990], sample #SA-78.

spectra of the Mauna Kea flow, suggesting that similar signatures could contribute to regional spectral signatures on Mars. Laboratory leaching experiments by *Yant et al.* [2016] showed that, after 14 days of leaching, the occurrence and strength of the concave-up and blue spectral slopes vary with both glass composition (e.g., mafic versus silicic) and pH.

Thus, the primary difference between near-infrared reflection spectra of well-developed residual leached rinds and silica coatings deposited without leaching is both a lack of silica or hydration absorption bands and the concave-up shape in the leached rind spectra. The lack of silica and hydration bands in the leached rind spectra is consistent with the leaching process being dominated by removal as opposed to deposition or exchange, as proposed by studies discussed above. However, the origin of the concave-up slope is unclear. The slope is typically fit well by an inverse power law function in wavelength, with an exponent between −2 and −4 [*Horgan and Bell*, 2012]. This function is similar to power law effects that occur due to Tyndall scattering in colloids [*He et al*., 2009], and similar spectral effects in the visible and near-infrared (VNIR) are observed due to scattering by submicron grains [*Brown*, 2014]. Thus, we hypothesize in this study that the concave-up spectral shape is due to wavelength-dependent scattering by structures at the submicron scale, perhaps related to surface textures or micron-scale porosity in the rinds.

An additional constraint on the origin of the concave-up slope comes from *Yant et al*. [2016], who showed that concave-up slopes are more prevalent in altered glasses that are both silica poor (basaltic) and have lower abundances of ferric iron (i.e., low Fe^{3+}/Fe_T ratio). This suggests that the dominant location of iron in the structure of the glass, either ferrous iron as a network-modifying ion or ferric iron as a network-forming ion, has an impact on the formation of the concave slope, perhaps via textural effects of leaching as discussed above.

In the midinfrared or thermal infrared (5–50 μm), emission dominates over reflection on planetary surfaces, and leached rinds and thin coatings are thin enough that thermal photons emitted from the unaltered substrate could potentially penetrate the rind or coating. However, laboratory studies of depositional silica coatings have shown that even very thin coatings (<10 μm) dominate the resulting thermal infrared (IR) spectra and entirely obscure the substrate [*Kraft et al*., 2003]. Spectra of silica coatings strongly resemble high-silica glasses like obsidian [*Kraft et al*., 2003; *Michalski et al*., 2006], although their absorption features are shifted relative to these phases. However, the thermal infrared spectral character of leached rinds is unclear. Thermal IR spectra of the natural Hawaiian leached samples in *Minitti et al*. [2007] also appear similar to high-silica glass, but as the thermal IR spectra reported are that of the bulk rock surface and not individual spots like in the near infrared, it is unclear what the contribution of leached rinds is to these spectra.

3. Methods

3.1. Acid Leaching Experiments

Four samples were used in this study, with varying degrees of crystallinity: a Columbia River Plateau basalt from the Rosa dike (BAS205), a partially glassy or hypocrystalline (crystals embedded in a glassy matrix) Icelandic olivine basalt from a subaqueous pillow lava (ICE170), a Hawaiian glassy basalt from a subaerial flow (BAS101), and Hawaiian basaltic glass sand, produced during explosive quenching of a lava flow entering the ocean and concentrated on a black sand beach (BSB101; see Tables 1 and 2 for sample information). Grain size is an important factor in weathering, so each basalt hand sample was both cut into centimeter-scale

Table 2. Major Oxides for Samples, Derived From X-ray Fluorescence (XRF)[a]

	BAS205[b] (wt %)	ICE170 (wt %)	BAS101 (wt %)	BSB101 (wt %)
SiO_2	51.6	46.4	50.6	49.5
TiO_2	3.13	0.75	3.19	2.15
Al_2O_3	13.2	14.4	13.1	12.7
Fe_2O_3	n.d.	11.0	1.07	2.66
FeO	14.4	8.39	10.6	8.84
MnO	0.23	0.17	0.18	0.17
MgO	4.59	13.0	6.38	9.51
CaO	8.55	13.4	10.7	9.76
Na_2O	2.90	1.35	3.05	1.99
K_2O	1.29	0.02	0.54	0.36
Total	99.9	100.5	99.4	97.6

[a]No chemical data are available for ICE170.
[b]*Atkinson* [1990], sample #SA-78.

fragments using a diamond rock saw and ground into sand (500–1000 μm) using a mortar and pestle. The centimeter-scale fragments exhibit both porous natural weathered surfaces and smooth fresh-cut surfaces. The basaltic glass was collected in the field as sand, so no centimeter-scale fragments are available.)

For our experiment, we have chosen to recreate an open hydrologic system, which we simulated by placing our samples in oxidizing and acidic solution baths and then frequently replacing the fluids with a fresh acid solution. Two stock acid solutions were made up using concentrated H_2SO_4 and distilled H_2O, with a pH of 1.0 (Acid A) and 3.0 (Acid B). Approximately 7 g of the four granular samples and the three cut samples was placed in separate Teflon vessels with 30 mL of the stock sulfuric acid solution and 10 mL of 30% H_2O_2—an instantaneous water:rock ratio of 5. Sulfuric acid was chosen as the acid for these experiments both based on the prevalence of this acid in the Martian geologic record [e.g., *Bibring et al*., 2006; *Hurowitz et al*., 2010] and in order to conform with previous experiments as discussed above. Hydrogen peroxide was chosen as the oxidizing agent because superoxides and peroxides have been suggested as candidates for the purported oxidant in Martian surface materials [*Zent and Mckay*, 1994; *Golden et al*., 2005; *Hurowitz et al*., 2007]. The consequences of including an oxidizing agent in this type of experiment are unclear, as similar precipitates were observed in experiments both with and without an oxidizing agent [*Golden et al*., 2005; *Tosca et al*., 2004]. The samples were fully immersed in the solutions initially for one day at a time, and gradually for longer durations as the alteration progress slowed. In total, all samples were exposed to acid for 213 days at 25°C, for a total additive water:rock ratio of approximately 100. Figure 1 shows an example of the sand-sized glassy basalt (BAS101), before immersion and after 69 days of leaching in Acid A (starting pH ~ 1). The grains exhibit white-colored coatings or rinds and possible pitting, both indications of surface weathering.

3.2. Near-Infrared Spectroscopy

Initial diffuse reflectance spectral data were collected as a baseline from all the samples using an ASD FieldSpec Pro HR spectrometer over the wavelength range of 0.35 to 2.5 μm. A 150 W quartz tungsten halogen light source was used to illuminate the samples and reflectance spectra were measured at $i = 30°$, $e = 0°$; 200 spectra were collected and averaged to improve SNR. To reduce the effects of specular reflections, all 500–1000 μm samples were spun on a turntable at 33.5 rpm during data collection. Some spectral signatures may still be attributable to diffraction effects related to specular reflection off of the ground glass sand samples, as shown by wavy spectra at visible wavelengths in Figure 5 (BAS101 Acid A).

On the days scheduled for spectra collection, the pH of each solution was recorded and the acid was decanted into an evaporation dish for future analysis. In order to remove all loose alteration products (i.e., all alteration products other than coatings or rinds), the decanted samples were rinsed with distilled H_2O and dried at 80°C for 2 h prior to spectral analysis. To ensure consistency, the same procedures used to collect the baseline spectra were implemented during each spectral measurement. Following data collection, a few grains of each sample were also set aside for future analysis. A fresh solution of acid and H_2O_2 was then prepared, the pH was recorded, and the samples were again placed in the solution.

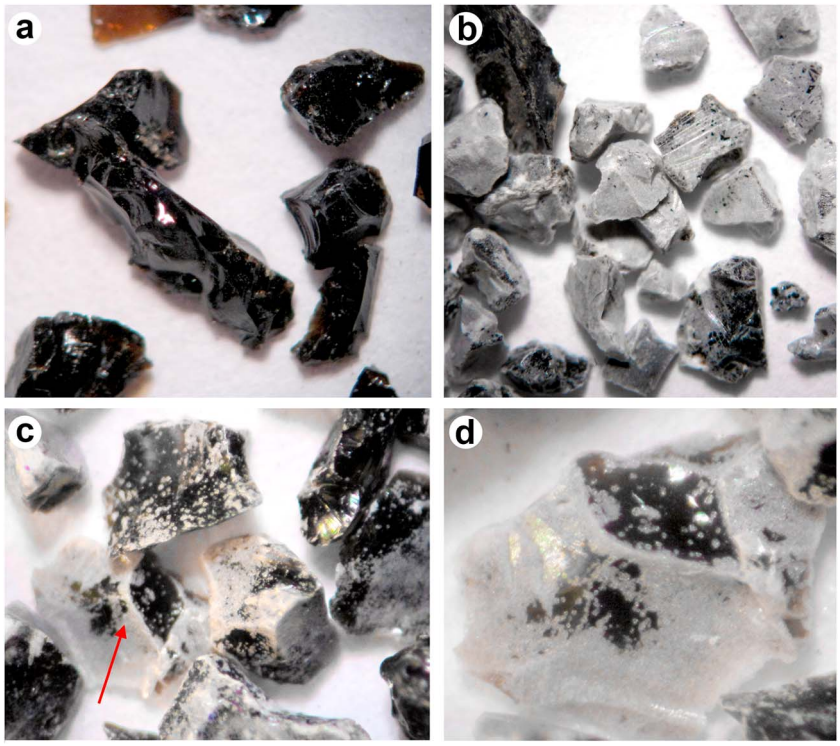

Figure 1. Visible microscope images of Hawaiian glassy basalt BAS101 ground sand samples; all grains are 500–1000 μm in diameter. (a) Before immersion in acidic solutions. (b) After 69 days of leaching in Acid A, under diffuse lighting. (c) After 69 days of leaching in Acid A, under directed lighting. Arrow indicates location of grain with possible pitted textures. (d) Close-up of the grain indicated by the arrow in Figure 1c.

3.3. Thermal Infrared Spectroscopy

Thermal infrared (TIR) emission spectra were measured at the Arizona State University Mars Space Flight Facility using a Nicolet Nexus 670 spectrometer that is configured to measure emissivity [*Ruff*, 1999]. Spectra were collected at a spectral resolution of 2 cm^{-1} over the range of 200–2000 cm^{-1}. Samples were placed in copper cups coated with black paint to achieve near-unit emissivity. The cups and samples were heated to 80°C for multiple hours prior to being measured, and this temperature was maintained during spectral acquisition by actively heating the sample with a hot plate. All TIR spectral measurements were taken after the acid leaching experiments were complete. TIR spectra were acquired for unaltered starting materials, end-stage materials (213 days of alteration), and select intermediate samples removed at various stages during the experiment.

Mineral abundances were estimated for sand-sized samples by modeling the TIR spectra using a spectral library of potential phases (Table 3), including common basalt minerals and weathering products, and a blackbody spectrum to obtain a nonnegative linear least squares fit to each measured spectrum [*Ramsey and Christensen*, 1998; *Rogers et al*., 2007]. End-members were chosen based on multiple parameters including spectrum quality, sample quality, and sample size—selecting coarse particulate or hand samples when possible. The detection limit for the linear deconvolution method ranges between 5% and 10% [*Feely and Christensen*, 1999], and the quality of the model is quantified by the RMS error, a parameter that compares the modeled emissivity spectrum to the measured spectrum [*Ramsey and Christensen*, 1998]. In general, a lower RMS value indicates a better fit, though the model should also be visually inspected for quality. Additionally, it is possible for the algorithm to select phases not present in the sample to substitute for end-members that are not available in the spectral library [e.g., *Ruff et al*., 2006].

Some physical properties of natural and laboratory samples are known to influence a spectrum such that the materials combine in ways that are not necessarily linear, and so they should be considered when analyzing modeled mineral abundances. Relatively thin (~10 μm) silicate weathering rinds and coatings can significantly contribute to and sometimes completely obscure the TIR signature of a surface [*Kahle et al*., 1988;

Table 3. Thermal Infrared Spectral End-Member Library

Mineral Group	End-Member
Alkali feldspar	Microcline CUR-3460A
Plagioclase	Albite WAR-0235
	Andesine WAR-0024
	Anorthite BUR-340
	Bytownite WAR-1384
	Labradorite BUR-3080A
	Oligoclase BUR-060
Orthopyroxene	Bronzite NMNH-93527
	Enstatite HS-9.4B
	Hypersthene NMNH-B18247
High-Ca clinopyroxene	Augite NMHN-93527
	Augite NMHN-9780
	Diopside WAR-6474
	Hedenbergite manganoan DSM-HED01
Low-Ca clinopyroxene	Avg. Lindsley pigeonite
Olivine	Fayalite WAR-FAY01
	Forsterite AZ-01
	KI3008Fo10
	KI3373Fo35
	KI3362 Fo60
	KI3115 Fo68
Phyllosilicates	Montmorillonite (Ca) STx-1
	Montmorillonite (Na) Swy-2
	Saponite $< 0.2\ \mu m$
	Serpentine HS-8.4B
	Smectite Swa-1
Sulfate	Anhydrite S16
	Coquimbite/paracoquimbite S46
	Gypsum S6
	Kieserite
Zeolite	Crystalline heulandite
	Crystalline stilbite
Carbonate	Calcite C40
	Dolomite C20
Oxide	Hematite BUR-2600
	Ilmenite WAR-4119
	Magnetite WAR-0384
	Titanomagnetite
Amorphous aluminosilicate	Allophane Si:Al 0.58 ALL0058[a]
	Aluminous opal
Amorphous silica	Opal A
	Opal CT
Felsic volcanic glass	Dacite glass MEM-4
	K-rich glass (obsidian)
	SiO_2 glass
Mafic volcanic glass	TES basalt proxy glass MEM-1

[a] *Rampe et al.* [2012].

Crisp et al., 1990; *Kraft et al.*, 2003; *Minitti et al.*, 2007], and thus, the abundance of such phases can be overestimated. Additionally, spectral contrast decreases with particle size, and so mineral mixtures of various particle sizes can cause certain phases to be overestimated or underestimated [*Rogers et al.*, 2007].

3.4. Scanning Electron Microscopy

In order to perform detailed microscopic analyses of the weathered particles, we randomly selected three grains of BAS205, ICE170, BSB101, and BAS101 starting materials and 10 grains of each corresponding ending material for scanning electron microscope (SEM) analysis. Grains were aligned on double-sided tape and then encapsulated in a two-part epoxy cured at room temperature. The sample stub was polished to 0.25 μm using progressively smaller-sized particle diamond suspension and diamond paste in order to get a cross-sectional view through the grains. The sample stub was carbon coated and then examined at the Arizona State University Center for high-resolution electron microscopy using an XL-30 SEM. The coating/rind thickness and morphology were examined using secondary electron (SE) and back-scattered electron imaging. Qualitative chemistry was measured using spot and line analyses as well as elemental maps obtained from the energy-dispersive X-ray spectroscopy system on the SEM. All SEM measurements were made at a working distance of 11 mm, an accelerating voltage of 20 kV, and a spot size of 3 or 4.

4. Near-Infrared Spectra

We observe four key types of near-infrared spectral changes during acid alteration of our basalt, glassy basalt, and basaltic glass samples, as summarized in Figure 2. These changes are almost all observed exclusively at pH ~ 1, as we find very little near-infrared spectral evidence for alteration of the residual primary grains by pH ~ 3 fluids. First, we observe changes to the relative strength of broad absorptions near 1 and 2 μm due to primary, iron-bearing minerals and glasses. This includes both the weakening of these iron bands overall and the strengthening of some iron bands relative to others (usually pyroxene absorptions at the expense of olivine absorptions). Second, we observe the appearance and sometimes the disappearance of narrow absorption bands near 1.4, 1.9, 2.2, and 2.4 μm, consistent with the deposition (and sometimes the removal) of various alteration minerals (e.g., silica, hydrated glass, gypsum, and other sulfates). Third, we observe a flattening of spectra at short visible wavelengths (typically between 0.4 and 0.7 μm), perhaps related to dissolution of fine-grained oxides. Lastly, we observe the development of strong spectral slopes in glassy samples, most likely related to

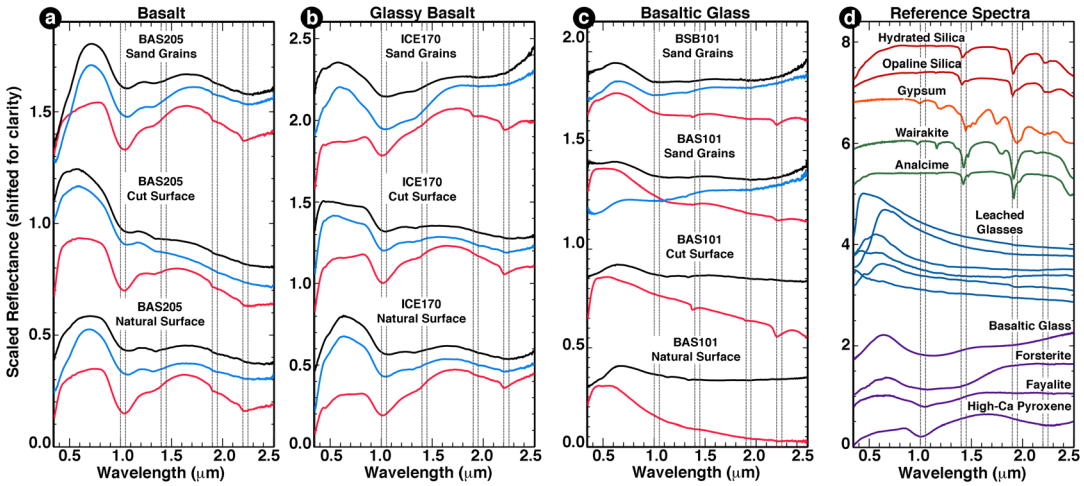

Figure 2. Summary of visible/near-infrared spectral results, showing spectra of glass and basalt samples before and after 213 days of alteration. Black spectra are from before alteration, blue are after alteration in Acid B (starting pH ~ 3), and red are after alteration in Acid A (starting pH ~ 1). (a) BAS205 crystalline basalt, (b) ICE170 partially glassy basalt, and (c) BAS101/BSB101 basaltic glasses, compared to (d) laboratory spectra [e.g., *Clark et al*., 2007] of primary minerals (purple), zeolites (green), sulfates (orange), and silica (red) and naturally altered glasses (blue) [*Minitti et al*., 2007]. Dashed lines indicate key absorption features in some spectra at 1.00, 1.05, 1.40, 1.45, 1.90, 1.95, 2.20, and 2.25 μm.

the development of rinds and coatings on the samples. We find that increasing spectral change correlates with both increasing acid strength and decreasing crystallinity. These results are detailed in the following section.

4.1. Basalt Samples

Spectra of crystalline Columbia River basalt (BAS205) are shown in Figure 3. Prior to alteration, the BAS205 samples all exhibit broad absorptions bands with minima near 1.05–1.07 μm, consistent with olivine, high-Ca pyroxene, or a mixture of the two [e.g., *Adams*, 1968; *Cloutis and Gaffey*, 1991]. Some samples also exhibit a second broad absorption near 2.2 μm, consistent with a high-Ca pyroxene component, which is strongest in the sand-sized samples. A strong shoulder on the 1 μm band near 1.3 μm suggests a contribution from olivine, which exhibits a shoulder at this location that is often apparent in mixtures [e.g., *Horgan et al*., 2014]. The depth of the 1.3 μm shoulder without a corresponding ~0.85 μm olivine shoulder may be enhanced by Fe-bearing plagioclase feldspar, which exhibits a band near 1.3 μm that is usually only visible for high ratios of plagioclase to pyroxene and olivine [e.g., *Cheek and Pieters*, 2014]. This primary mineral assemblage of significant plagioclase with lesser amounts of olivine and pyroxene is supported by thermal infrared spectral analysis (section 5).

As exposure time progresses, the acids appear to have limited or no effect on the spectra of the rinsed basalt samples, with Acid B (starting pH ~ 3) causing no apparent spectral changes. All BAS205 samples exposed to Acid A (starting pH ~ 1) do exhibit a strengthening of the 1 and 2 μm bands, without a concomitant increase in the strength of the 1.3 μm olivine/plagioclase shoulder. We hypothesize that the overall strengthening of the bands is due to either exposure of larger grains and/or the preferential dissolution of opaque components, such as those that may be present as a fine-grained matrix. The fact that the 1.3 μm shoulder band depth remains relatively unchanged could be consistent with a preferential dissolution of olivine, but not plagioclase, relative to pyroxene, resulting in spectra dominated by pyroxene signatures. In addition, Acid A causes a significant flattening of the spectra of all samples between 0.45 and 0.70 μm, perhaps also consistent with the removal of fine-grained, Fe/Ti oxide-bearing matrix materials. Lastly, Acid A also causes the appearance of very weak narrow absorption bands near 1.9 and 2.2 μm, likely due to small amounts of hydrated silica. It is key to note that surface texture and grain size appear to have no influence on observed spectral changes in this crystalline basalt, unlike many of the samples discussed below.

4.2. Glassy Basalt Samples

Spectra of the glass-bearing Icelandic pillow basalt (ICE170) are shown in Figure 4. Prior to alteration, most of the ICE170 samples exhibit broad absorption bands with minima near 1.05 and 2.2 μm that are consistent with a high-calcium pyroxene, with a contribution from olivine, as indicated by a strong shoulder near

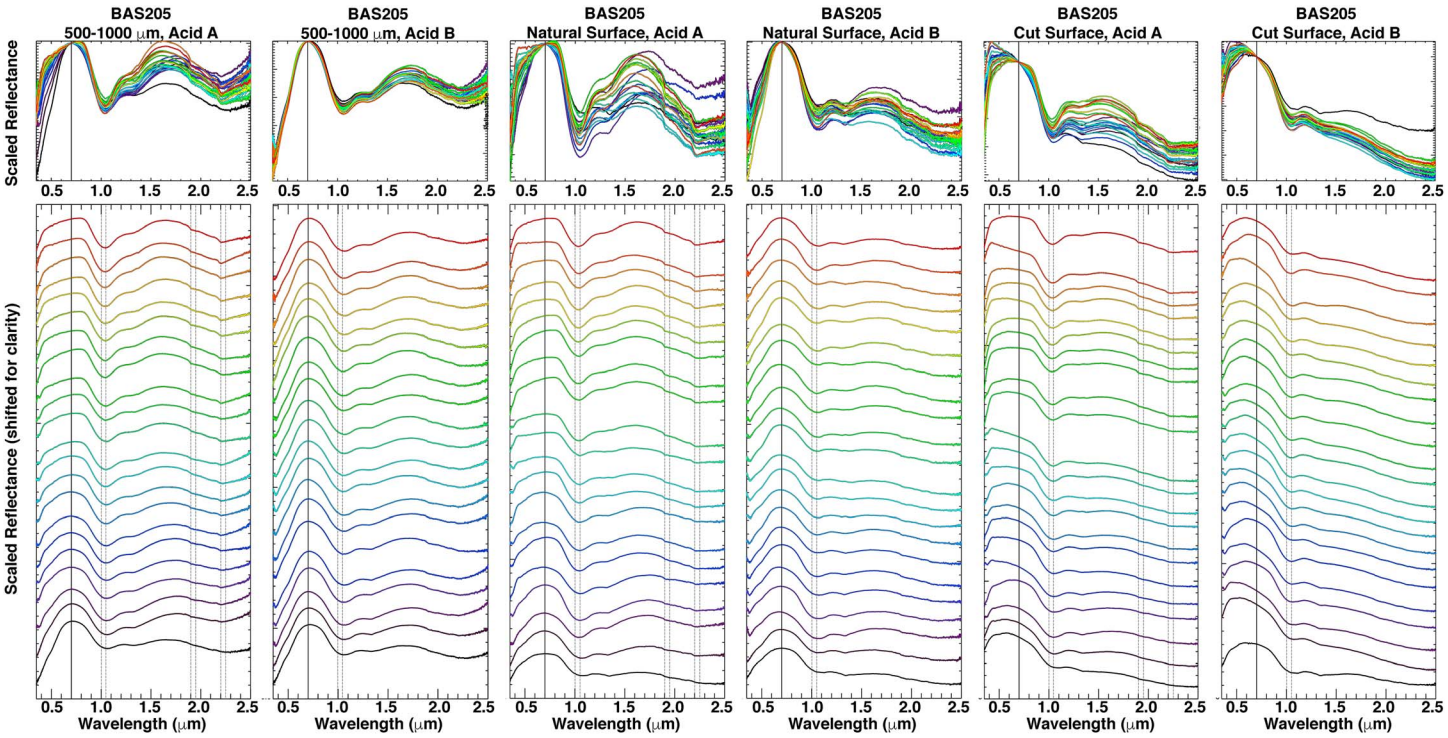

Figure 3. Near-infrared spectra of Columbia River flood basalt sample BAS205 before, during, and after 213 days of leaching (from bottom to top, days 0, 1, 2, 3, 4, 6, 8, 10, 13, 16, 20, 23, 29, 36, 43, 50, 59, 69, 83, 101, 122, 213). All spectra have been normalized near 0.6 μm, as shown in the top row. The bottom row shows these same spectra stacked for clarity, with dashed lines for reference shown where needed at 1.00, 1.05, 1.40, 1.45, 1.90, 1.95, 2.20, and 2.25 μm. Anomalous spectra not shown: 500–1000 μm Acid B day 59 and natural surface Acid A day 13.

1.25 μm and a corresponding weaker shoulder near 0.85 μm. These absorptions are demonstrated most clearly in the sand-sized samples. However, there is variability within the starting samples. The cut surfaces of the larger samples exhibit both more subdued olivine absorptions and a flattening in the visible compared to the sand-sized sample, which we hypothesize is due to lower spectral contrast in the slab. The natural surface of the sample exposed to Acid A exhibits absorptions centered near 1.05 and 2.25 μm consistent with pyroxene; however, the 1 μm band has an asymmetrical shape due to additional absorption at longer wavelengths. While this could be consistent with an olivine component, the lack of the corresponding ~0.85 μm feature observed in the other, likely olivine-bearing samples suggests that this asymmetry is instead due to iron-bearing glass, which exhibits an iron absorption band centered at longer wavelengths (1.1–1.2 μm). The spectrum of the natural surface of the sample exposed to Acid B clearly exhibits a broad, glass-like 1 μm absorption band centered closer to 1.12 μm. The presence of glass on the natural surface is consistent with a glassy quench rind on this pillow lava.

Acid B (starting pH ~ 3) has very little effect on the spectra of the sand grains and the cut surface of the Icelandic basaltic pillow lava, with virtually no clear difference between the spectra of the cut surface from day 0 and day 213 (Figure 4). Notably, the sand grains still exhibit a strong olivine signature at the end of the experiment, which may be somewhat stronger than the starting sample, perhaps due to some preferential loss of pyroxene. The natural glassy quench rind surface does exhibit significant variability throughout exposure to Acid B—at various stages exhibiting absorption bands consistent with olivine, pyroxene, or glass. We interpret this variability to represent heterogeneity in the sample, either due to concentrations and/or phenocrysts of these phases being exposed by the acid over time or due to the rough surface texture and variation in the precise viewing geometry emphasizing some phases over others in subsequent spectra. However, the spectra of the natural surface eventually stabilize, exhibiting absorption bands and an overall shape that are very similar to the spectra of the cut surface.

In contrast, all Icelandic pillow basalt samples (ICE170) exposed to Acid A (starting pH ~ 1) exhibit clear spectral signatures of alteration. As soon as days 2–4, all samples exhibit weak absorption bands near

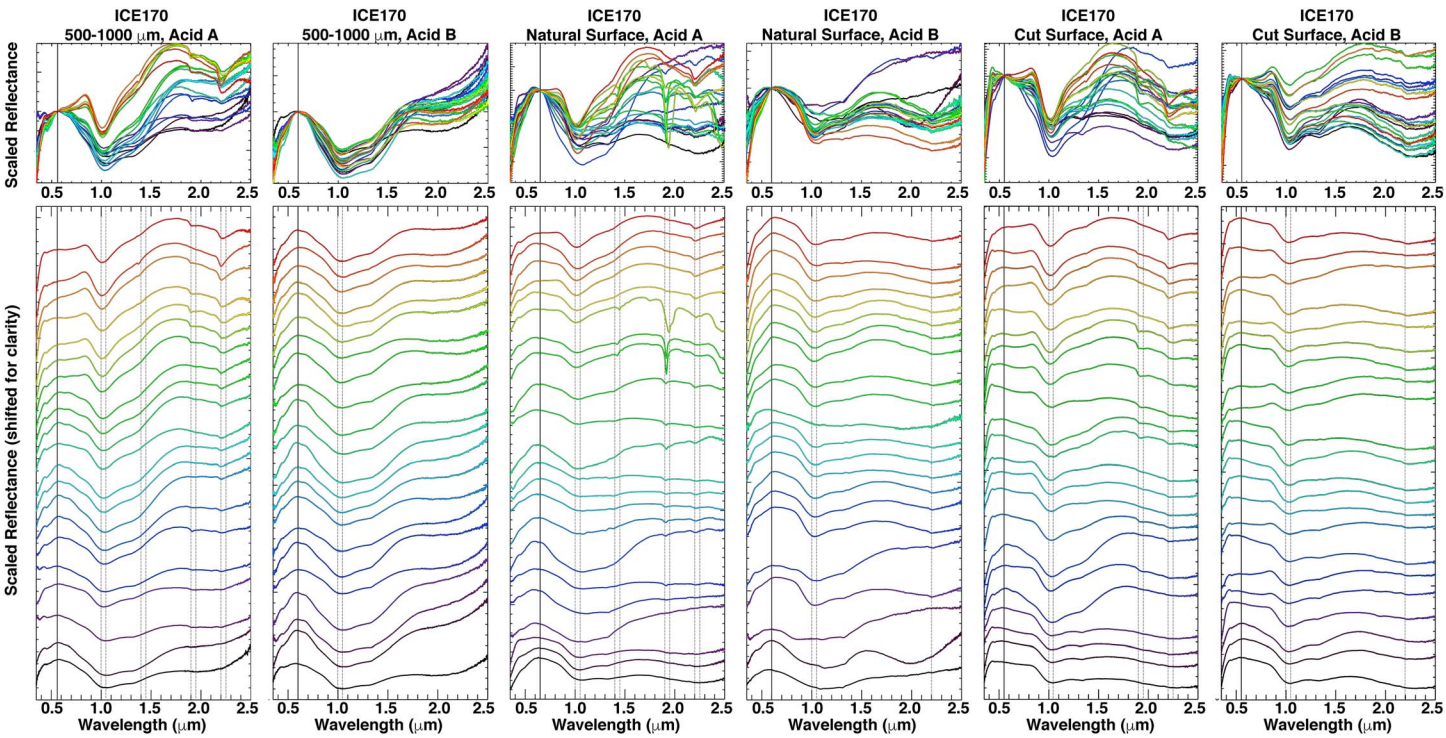

Figure 4. Near-infrared spectra of Icelandic glass-bearing basalt ICE170 before, during, and after 213 days of leaching (from bottom to top, days 0, 1, 2, 3, 4, 6, 8, 10, 13, 16, 20, 23, 29, 36, 43, 50, 59, 69, 83, 101, 122, 213). All spectra have been normalized near 0.6 μm, as shown in the top row. The bottom row shows these same spectra stacked for clarity, with dashed lines for reference shown where needed at 1.00, 1.05, 1.40, 1.45, 1.90, 1.95, 2.20, and 2.25 μm. Missing spectrum not shown: 500–1000 μm Acid A day 69.

1.9 and 2.2 μm. The 2.2 μm absorption deepens over the course of the experiment and develops an asymmetric shape with more absorption toward longer wavelengths. These spectral features are consistent with hydrated silica or hydrated glass, as shown in Figure 2, most likely present as a coating on the samples. The natural surface of the larger sample also exhibits transient spectral features near 1.45, 1.75, 1.95, 2.27, and 2.42 μm on day 59 that are consistent with the hydrated Ca sulfate gypsum, as shown in Figure 2. Additionally, on days 43 and 50, this same sample exhibits spectral features near 1.42, 1.92, 1.78, 2.1, and 2.46 μm that are most consistent with a combination of Al- and Mg-bearing sulfates (e.g., alunite and kieserite [*Cloutis et al.*, 2006]), as shown in Figure 2. All of these sulfates are known products of acid alteration [e.g., *Tosca et al.*, 2004; *Golden et al.*, 2005; *Marcucci and Hynek*, 2014]. The fact that they are only observed transiently on the natural surface of the larger sample suggests that we observed them because the rough surface texture temporarily prevented them from being removed during the rinsing step.

The final spectra of all three Icelandic pillow basalt samples (sand grains, natural surface, and cut surface) exposed to Acid A look remarkably similar. In addition to the narrow silica absorption bands near 1.9 and 2.2 μm, all three samples exhibit broad high-Ca pyroxene absorptions near 1.05 and 2.25 μm and a similar spectral shape. The 1 μm pyroxene absorptions have become clearer due to the loss of longer-wavelength olivine and glass absorptions, suggesting that preferential dissolution of olivine and glass occurred on the grain and sample surfaces. Finally, similar to the crystalline basalt samples, alteration by Acid A tends to flatten the spectra in the short wavelengths, in this case between 0.4 and 0.8 μm.

4.3. Glass Samples

Spectra of the glass-rich Hawaiian basaltic lava (BAS101) and glass-rich pyroclastic beads (BSB101) are shown in Figure 5. Prior to alteration, the granular lava sample (BAS101) exhibits broad but shallow absorption bands near 1.15 and 1.95 μm that are classic examples of iron absorptions in glass [e.g., *Adams et al.*, 1974; *Minitti et al.*, 2002]. The pyroclastic bead sample (BSB101) exhibits similar bands, but with additional absorption within the 1 μm band near 1.05 and 1.3 μm consistent with some degree of recrystallization to olivine within the glass.

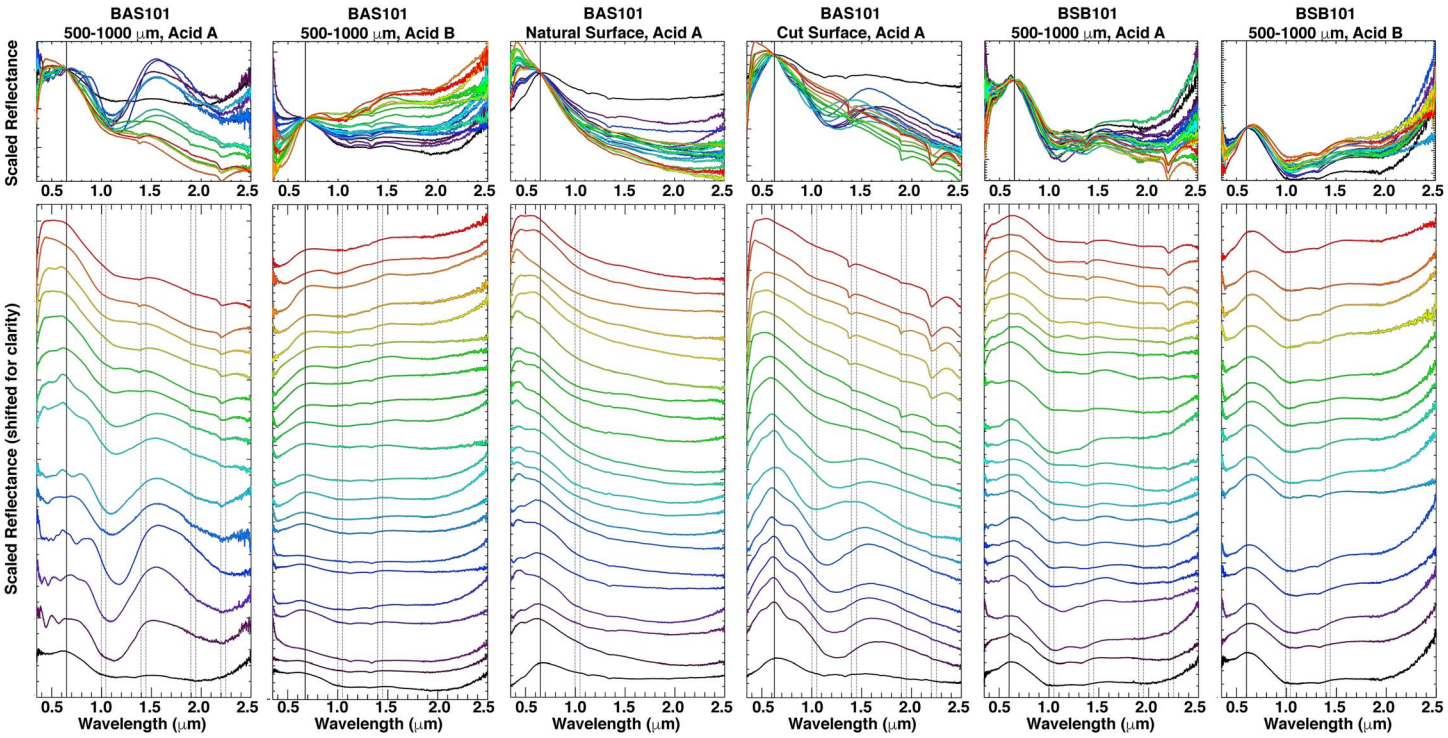

Figure 5. Near-infrared spectra of Hawaiian glass-rich samples—glassy basalt sample BAS101 and glass sand sample BSB101—before, during, and after 213 days of leaching (from bottom to top, days 0, 1, 2, 3, 4, 6, 8, 10, 13, 16, 20, 23, 29, 36, 43, 50, 59, 69, 83, 101, 122, 213). All spectra have been normalized near 0.6 μm, as shown in the top row. The bottom row shows these same spectra stacked for clarity, with dashed lines for reference shown where needed at 1.00, 1.05, 1.40, 1.45, 1.90, 1.95, 2.20, and 2.25 μm. Possible diffraction effects are apparent in BAS101 Acid A grains before day 36, although the strongest diffraction-obscured or otherwise anomalous spectra are not shown: BAS101 500–1000 μm Acid A days 1, 2, 4, 6, 8, 16, 20, and 29; BAS101 natural surface day 23; and BAS101 cut surface days 1, 2, 8, and 10.

On alteration in Acid B (starting pH ~ 3), these absorption bands in all samples remain unchanged throughout the experiment, and no silica or hydration bands are observed. However, both granular samples develop a strong red slope (reflectance increasing to longer wavelengths) and additional absorptions near 0.5 μm, which together are most consistent with an oxide coating [e.g., *Fischer and Pieters*, 1993].

On exposure to Acid A (starting pH ~ 1), the granular glassy samples exhibit nearly opposite behavior from Acid B. In both samples, the glass absorptions initially appear to strengthen significantly. In both samples, diffraction effects die out as the 1 and 2 μm bands become subdued. In the final spectra, while the 1 μm band is still clearly visible, the 2 μm band has largely disappeared in both samples. The olivine absorptions in the beads (BSB101) also have disappeared, leaving a symmetric shape centered near 1.1 μm that is much more consistent with glass. Over the course of the experiment, both granular samples develop a strong concave-up slope (greater blue slope at shorter wavelengths). This shape is characteristic of leached rinds that have been shown to form on natural glass samples due to acid leaching, as discussed above (sections 2.2 and 2.3). The lava grains (BAS101) also develop a strong blue slope (decreasing reflectance at longer wavelengths) that is most apparent at longer wavelengths (1.5–2.5 μm). Both granular samples develop narrow absorptions near 1.38 and 2.20 μm, consistent with hydrated silica or hydrated glass.

Prior to alteration, the natural surface of the glass-rich lava (BAS101) already exhibits a weak concave-up slope characteristic of leached glassy rinds, without any absorptions due to glass, olivine, hydration, or any alteration phases. Over the course of the experiment, the strength of the concave-up slope gradually increases, and the short visible wavelengths also flatten out, as observed in the granular sample. Like in the BAS101 Acid A grains, the slope is blue as well as concave. No absorption bands are observed to form in the natural surface spectra throughout the experiment.

The cut surface exhibits very different spectral characteristics from any other sample, both initially and throughout the experiment. The cut surface initially only exhibits a weak glass band near 1.15 μm with no corresponding 2 μm band, superposed on a weak linear (nonconcave) blue slope. With exposure, the glass

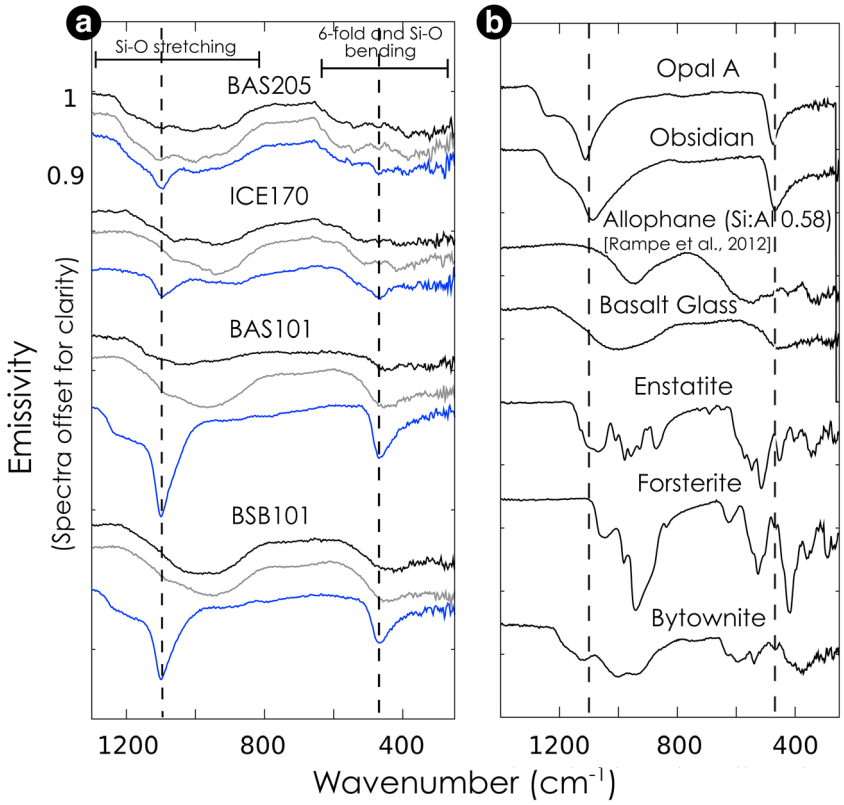

Figure 6. (a) Thermal infrared spectra of all sand-sized samples. Black spectra indicate starting material, gray spectra indicate grains weathered in Acid B (starting pH 3) for 213 days, and blue spectra indicate grains weathered in Acid A (starting pH 1) for 213 days. Vertical dashed lines indicate emissivity minima at 1100 and 465 cm^{-1} for the materials weathered in pH 1 acid. (b) Laboratory spectra from the Arizona State University Online Spectral Library Tool, showing examples of some of the end-member phases in Table 3. Vertical dashed lines indicate emissivity minima positions at 1100 and 465 cm^{-1} for the materials weathered in pH 1 acid.

band appears to strengthen, and while some of this may be due to diffraction, some of the increase may be real, as the day 59 spectrum exhibits no apparent diffraction but does exhibit very strong glass bands. Eventually, the glass bands are completely subdued. This is most likely due to the development of a hydrated silica coating, as suggested by both the strong blue slope of the altered spectra and the strong absorptions near 1.38, 1.9, and 2.2 μm.

5. Thermal Infrared Spectra

In general, we see changes in the thermal infrared spectral shape in two main wavenumber regions for the acid-leached basalt, glassy basalt, and basaltic glass samples, as summarized in Figure 6. As with the near infrared, the spectral changes are observed almost exclusively at pH ~ 1, and there is little spectral evidence for alteration of the primary grains by pH ~ 3 fluids. The first spectral change is a shift of the emissivity minimum in the wavenumber range of the fundamental Si–O asymmetric stretching vibration between ~900 and 1300 cm^{-1}, suggesting that the weathering process is affecting the silicate structure of the samples. When exposed to Acid A, most samples show emissivity minima shifted to a higher wavenumber (~1100 cm^{-1}), indicating increased polymerization of the material [*White and Minser*, 1984; *Crisp et al*., 1990; *Michalski et al*., 2005]. However, this emissivity minimum is lower than that of pure opal (1115 cm^{-1}), indicating that the material probably contains network-modifying cations (e.g. K^+, Na^+, and Mg^{2+}) and/or water molecules that cause the structure to depolymerize. Samples exposed to Acid B generally show emissivity minima shifted toward lower wavenumbers, which suggests a preferential loss of more polymerized phases, such as plagioclase (Figure 6).

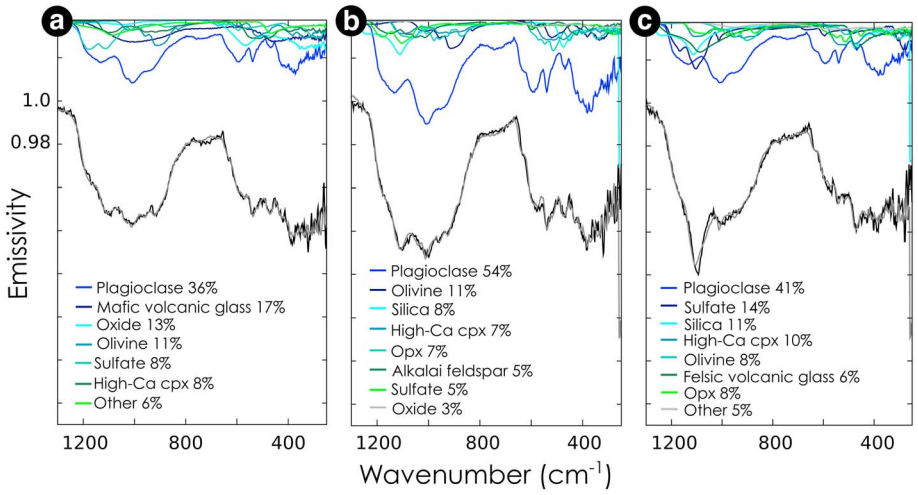

Figure 7. Linear deconvolution of thermal IR spectra of BAS205 (a) starting material, (b) grains exposed to Acid B, and (c) grains exposed to Acid A, using mineral end-member library in Table 3. The "Other" category is a bin for phases modeled in abundances < 5%. RMS error = 0.17%, 0.23%, and 0.22%, respectively. Black and gray indicate the measured and modeled spectra, respectively.

The second spectral change is a shift of the emissivity minimum between ~300 and 600 cm^{-1}. The absorptions in this region are more complicated for crystalline samples, because of overlap in the energy levels of tetrahedral Si–O bending vibrations as well as vibrations of cations in sixfold coordination sites [*Michalski et al*., 2005], and so each case is examined separately. However, in general, we see the development of a local emissivity minimum around 465 cm^{-1} in all samples exposed to Acid A, which can most likely be attributed to tetrahedral Si–O bending vibrations [*Lippincott et al*., 1958]. These observations are detailed in the following sections. The spectral differences between samples as they relate to microscale weathering features and starting material physical properties are discussed in our companion paper [*Smith et al*., 2017].

5.1. Basalt Samples

The two broad absorption features of the crystalline basalt (BAS205) starting material are centered near 1010 and 360 cm^{-1}, which are consistent with a mafic composition [*Feely and Christensen*, 1999; *Bandfield et al*., 2000]. The abundance of superposed high-frequency absorption features suggests the presence of crystalline phases (Figure 6). Linear unmixing suggests that BAS205 is predominantly composed of plagioclase feldspar, mafic glass, oxides (titanomagnetite), olivine, and high-Ca clinopyroxene (Figure 7).

The spectral changes to BAS205 grains after exposure to Acid B are very subtle. We observe an overall increase in spectral contrast with increasing alteration time at all wavenumbers, and especially between 880 and 1190 cm^{-1} (Figure 8). We also observe a decrease in the absorption feature centered at 918 cm^{-1} (Figure 8). These changes in the spectral shape are interpreted in the unmixing models as a relative increase in plagioclase and amorphous silicate/silica phases at the expense of mafic glass and oxides (Figure 7). In both Acid A and Acid B samples, the relative increase in primary phases (including plagioclase and pyroxenes) after alteration suggests that some material was totally lost to solution, rather than reprecipitated as an alteration product.

After exposure to Acid A for 4 days, the main Si–O stretching emissivity minimum of the granular samples shifts to 1100 cm^{-1}, while still retaining the local emissivity minimum at ~1010 cm^{-1} (Figure 8). After 29 days in Acid A, the overall spectral absorption shape becomes slightly broader at lower wavenumbers, the spectral contrast decreases between ~320–420 and 500–650 cm^{-1}, and a 465 cm^{-1} feature deepens. Around day 69, the 1100 cm^{-1} feature begins to deepen further so that at the end of the experiment at 213 days, the 1100 cm^{-1} feature is dominant. However, there still remains an absorption feature centered near 980 cm^{-1}, apparent as a shoulder on the main Si–O stretching absorption. The linear deconvolution model attributes these changes to a relative decrease in mafic glass and oxides and an increase in amorphous silicate/silica phases (including a felsic glass) and sulfate minerals (Figure 7). The sulfate minerals are most

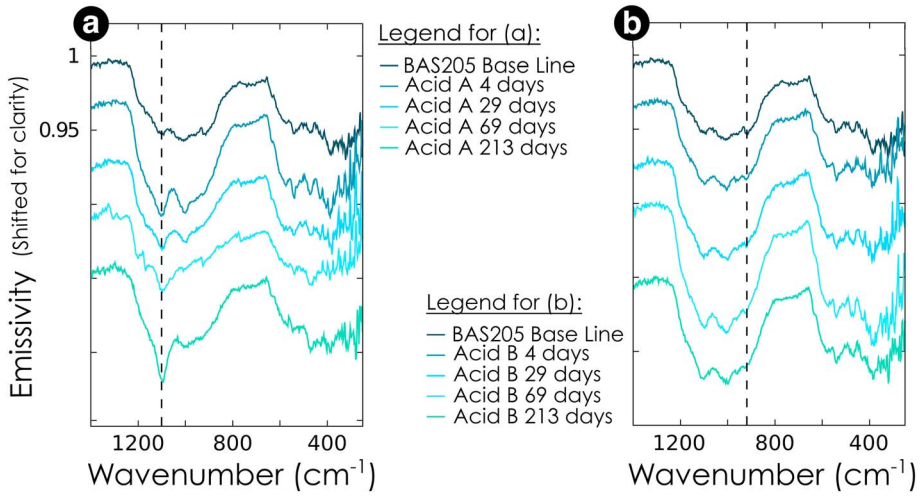

Figure 8. Thermal infrared spectral evolution of BAS205 grains exposed to (a) Acid A and (b) Acid B over the duration of the experiment. The dashed line in Figure 8a indicates 1100 cm^{-1}, the final location of the shifting Si–O stretching emissivity minimum. In Figure 8b, the dashed line is centered at 918 cm^{-1}, indicating a relative decrease in mafic glass and oxide abundances.

likely not actually present in the altered sample because their inclusion creates a sharp feature ~1020 cm^{-1} in the model that is not apparent in the measured spectrum.

5.2. Glassy Basalt Samples

ICE170 grains initially look similar to BAS205 starting material, but with slightly broader absorption features centered on 1000 and 400 cm^{-1} that can be attributed to a greater abundance of basaltic glass (Figure 6). This is evident in the linear deconvolution result that uses mostly basaltic glass, olivine, and pyroxene to model the measured spectrum (Figure 9).

The Si–O stretching emissivity minimum of ICE170 shifts to a higher wavenumber after exposure to Acid A for only 6 days (Figure 10). The spectral shape stays nearly the same until the end of the experiment at 213 days, when the sample develops sharp emissivity minima at 1095 and 465 cm^{-1} while retaining local minima centered around 925 and 380 cm^{-1} (Figure 10). These changes are modeled as an overall decrease in basaltic glass and a relative increase in high-silica phases such as phyllosilicates, amorphous silica, and zeolites, as

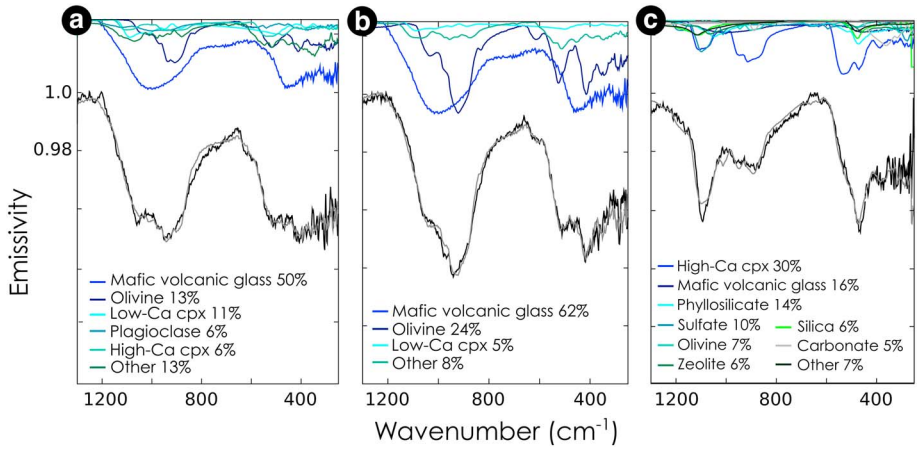

Figure 9. Linear deconvolution of thermal IR spectra of ICE170 (a) starting material, (b) grains exposed to Acid B, and (c) grains exposed to Acid A, using mineral end-member library in Table 3. RMS error = 0.22%, 0.24%, and 0.21%, respectively. Black and gray indicate the measured and modeled spectra, respectively.

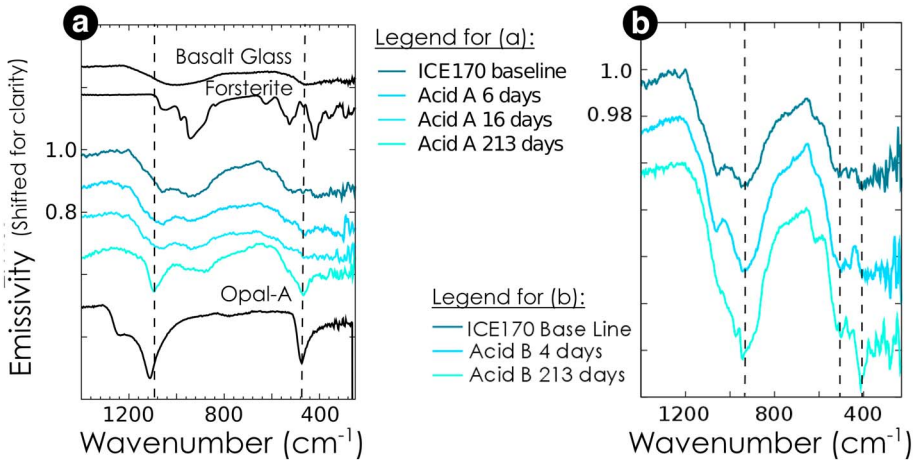

Figure 10. Spectral evolution of ICE170 grains weathered in (a) Acid A and (b) Acid B for the duration of the experiments. Black spectra are taken from the spectral library and are shown for comparison. Dashed lines indicate emissivity minima of final products from experiments at 1095 and 465 cm^{-1} (Figure 10a) and at 940, 510, and 415 cm^{-1} (Figure 10b).

well as sulfates (Figure 9). The dominant high-silica phase used to model the spectrum of the material after 213 days is montmorillonite, which has a Si–O stretching emissivity minimum at ~1070 cm^{-1}, yet there is no indication of clays in the near-IR spectra. Additionally, sulfates do not appear to be real components in the samples because their inclusion in the spectral modeling induces features at 1010 and 290 cm^{-1} that are not present in the data. Due to this sulfate misfit and the lack of near-IR clay or sulfate absorptions bands in this sample, we hypothesize that the model is using these high-silica and sulfate phases to replicate the spectrum of another high-silica end-member not present in our library. This phase appears to have a minimum near 1095 cm^{-1}, suggesting that it may be somewhat less polymerized than opaline silica. There is also a modeled increase in clinopyroxene, mainly at the expense of glass, but also due to some loss of olivine and plagioclase.

After exposure of ICE170 to Acid B for 4 days, the spectral feature at 940 cm^{-1} deepens significantly, becoming the dominant emission feature (Figure 10). There is little change to the spectrum until the end of the experiment at 213 days when a feature at 1060 cm^{-1} essentially disappears (Figure 10). At lower wavenumber, the sample retains the major absorption features of the starting material at 415 and 510 cm^{-1}, but the 415 cm^{-1} feature deepens greatly. These spectral changes are modeled as a relative increase in more mafic phases such as basaltic glass and olivine, at the expense or pyroxene and plagioclase (Figure 9). Notably, no significant alteration phases are detected; however, the Si–O stretching emissivity minimum shift to a lower wavenumber indicates that the sample has become more structurally disordered.

5.3. Glass Samples

The thermal IR spectra of the unaltered glass-rich Hawaiian basaltic lava (BAS101) and glass-rich pyroclastic beads (BSB101) are shown in Figure 6. Both spectra look very similar to a typical basaltic glass [e.g., *Crisp et al.*, 1990; *Farrand et al.*, 2016], with broad Si–O stretching and bending spectral features centered around 1010 and 445 cm^{-1} for the lava grains and ~980 and 430 cm^{-1} for the pyroclastic beads (Figure 6). The spectra also have very few superposed narrow absorption features, which suggests a high abundance of basaltic glass, and this interpretation is supported by the linear unmixing analysis (Figure 11). The glass-rich BSB101 sand samples have a wider Si–O stretching absorption feature shifted to a lower wavenumber than that of a typical basaltic glass (Figure 6), which suggests the presence of olivine and is supported by the linear unmixing model (Figure 13).

Both of the basaltic glass samples exposed to Acid B show Si–O stretching features shifted toward a lower wavenumber. BAS101 exposed to Acid B alters very slowly, remaining spectrally unchanged until near the end of the experiment at 213 days when a shallow absorption feature around 1060 cm^{-1} is lost, which shifts the center of the Si–O stretching absorption feature to a lower wavenumber (~970 cm^{-1}; Figure 12). Similarly, the Si–O stretching feature of BSB101 is shifted to ~960 cm^{-1} (Figure 6). At lower wavenumbers, the

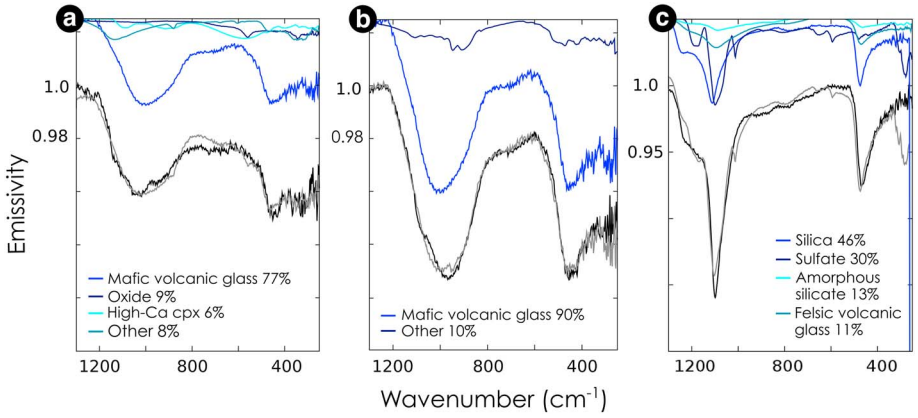

Figure 11. Linear deconvolution of thermal IR spectra of BAS101 (a) starting material, (b) grains exposed to Acid B, and (c) grains exposed to Acid A, using mineral end-member library shown in Table 3. The "Other" category is an additive bin for phases modeled in abundances < 5%. RMS error = 0.28%, 0.81%, and 0.26%, respectively. Black and gray indicate the measured and modeled spectra, respectively.

absorption feature ~450 cm^{-1} deepens for both samples, and a feature at ~340 cm^{-1} is almost completely removed from the BAS101 spectrum.

The spectral changes for BAS101 are represented in the unmixing model as a loss of clinopyroxene and relative increase in basaltic glass (Figure 11). The loss of the absorption feature at ~340 cm^{-1} possibly indicates a decrease in iron oxides. This could be consistent with the visible spectral character of BAS101 unaltered surfaces, which exhibit shallow but broad absorptions near 500 and 750 nm, the former of which could be consistent with magnetite. These absorptions vary in intensity during the experiment but are not apparent at the end of the experiment. In general, the shift of the emissivity minimum toward a lower wavenumber suggests that the sample has become more structurally disordered.

The spectral change for BSB101 grains exposed to Acid B for 213 days is not reflected in the abundances derived by the linear unmixing model, which remains unchanged from the unaltered materials; however,

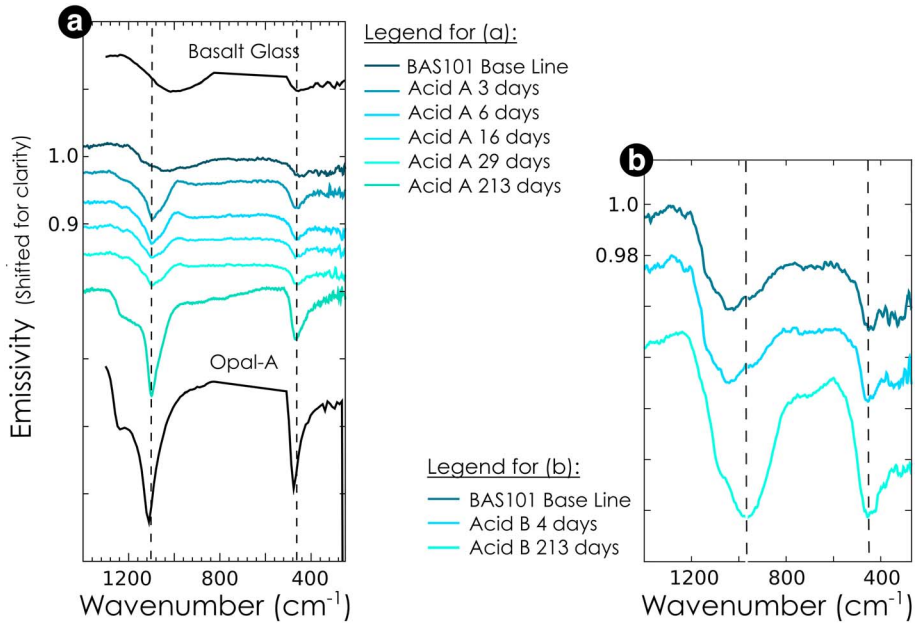

Figure 12. Thermal infrared spectral evolution of BAS101 grains exposed to (a) Acid A and (b) Acid B over the duration of the experiment. Black spectra are taken from the spectral library and are shown for comparison. Dashed lines indicate emissivity minima positions for final products from both experiments at 1100 and 465 cm^{-1} (Figure 12a) and at 970 and 450 cm^{-1} (Figure 12b).

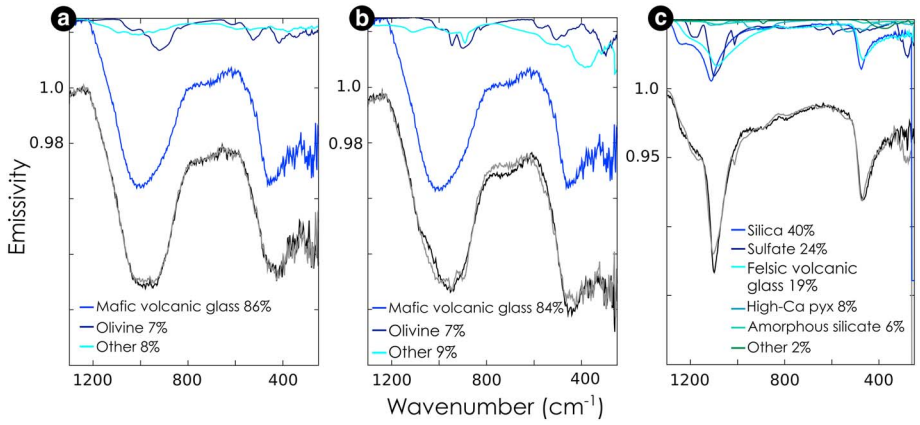

Figure 13. Linear deconvolution of TIR spectrum of BSB101 (a) starting material, (b) grains exposed to Acid B, and (c) grains exposed to Acid A, using mineral end-member library shown in Table 3. The "Other" category is an additive bin for phases modeled in abundances below the detection limit (<5%). RMS error = 0.15%, 0.42%, and 0.27%, respectively.

the misfit between the measured and modeled spectra is increased (Figure 13). The inclusion of olivine in the model induces features in the model at ~900 and 450 cm^{-1} that are not present in the measured spectrum of the altered glass. The BSB101 starting material is modeled with the same abundance of olivine without inducing spectral features, and so we can assume that olivine was actually present in the starting material but was preferentially lost when altered in Acid B (Figure 13).

Exposure of the basaltic glass samples to Acid A creates a much more drastic spectral change than for either of the more crystalline samples (Figure 6). After just 3 days in the acid, the Si–O stretching and bending absorption features of the lava grains become much more narrow and the minima shift to 1100 and 465 cm^{-1}. Additionally, a very shallow shoulder centered at 1220 cm^{-1} starts to develop (Figure 12). These features deepen over the time of the experiment, and the resulting spectral shape for both basalt glass samples is very similar to that of Opal A, but with emissivity minima at 1100 and 465 cm^{-1}, instead of 1115 and 470 cm^{-1} as would be expected for pure Opal A (Figure 6).

These spectral changes are represented in the unmixing model as a total replacement of the primary phases by secondary high-silica phases. As in ICE170 Acid A, we hypothesize that the spectral unmixing model uses a combination of amorphous silica/silicates, felsic volcanic glass, and sulfates to obtain the general spectral shape and correct wavenumber emissivity minima of an amorphous aluminosilicate end-member not present in our library (Figure 11). It is evident that sulfates are most likely not a component of the sample because of the misfit between the modeled and measured spectra at ~280 cm^{-1}. Therefore, the high-silica phase measured in these acid-altered basalt glass samples is not available in the current spectral library. Felsic volcanic glass is frequently used in TIR spectral modeling of Surface Type 2 regions on Mars, so its inclusion in the models here is worth noting (Figures 11 and 13).

The resulting spectral shapes of the basaltic glass samples altered in pH 1 acid look very similar to basaltic glasses naturally weathered in acidic environments [*Minitti et al.*, 2007]. For example, naturally weathered Hawaiian basaltic glasses from the Mauna Iki flow (MIO) and from near the outgassing Halemaumau vent at Kilauea (KWY and KW) also have Si–O stretching emissivity minima between 1087 and 1100 cm^{-1}, Si–O bending emissivity minima between 450 and 170 cm^{-1}, and spectral shoulders ~1220 cm^{-1} [*Kahle et al.*, 1988; *Crisp et al.*, 1990; *Minitti et al.*, 2007]. *Minitti et al.* [2007] performed SEM and electron microprobe analyses on the samples and found that the distinct spectral signature was coming from leached rinds coated with layers of silica-rich material. *Crisp et al.* [1990] studied samples from Hawaiian lava flows of varying age and found that lava flows exhibit similar spectral features when they are greater than a few years old. They attributed the spectral features to the accumulation of silica-rich depositional coatings over time. Our companion paper found silica-rich layers on the basalt glass sand samples in this study, and so we also assign the combination of ~1100, 465, and 1220 cm^{-1} features to silica-rich alteration layers [*Smith et al.*, 2017].

The 1220 cm^{-1} shoulder on the deeper 1100 cm^{-1} absorption band is found in many silica-rich glasses and silica-rich amorphous alteration phases and represents one of two states of the SiO_2 asymmetric stretching

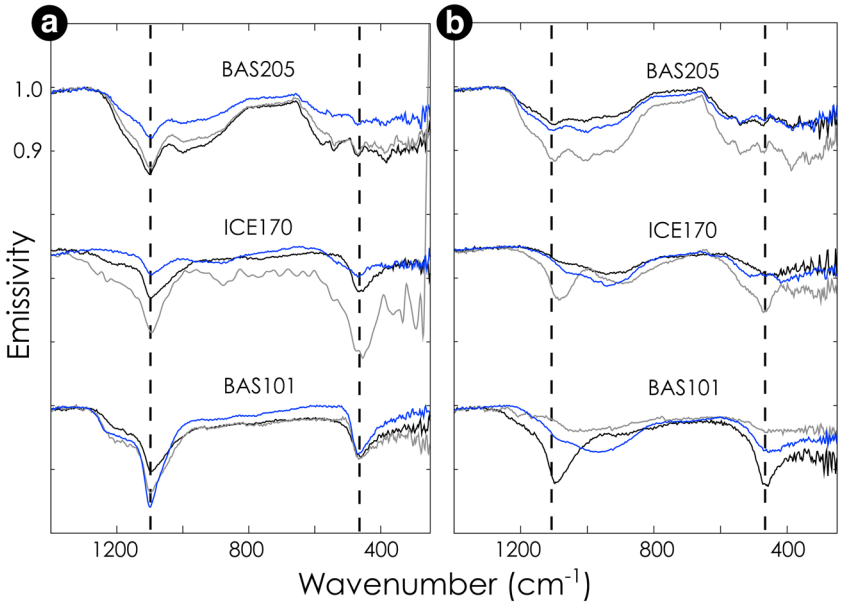

Figure 14. TIR spectra of altered oriented fragment surfaces for samples weathered in (a) Acid A and (b) Acid B. Naturally textured surfaces (black lines) of these fragments are spectrally similar to the equivalent sand grain spectra (blue). However, the artificially smooth cut surfaces (gray) exhibit much deeper silica absorption bands. This is especially true in moderate-pH experiments, even though silica coatings were not observed on either the sand grains or natural surfaces. Dashed lines in both plots indicate the position of the shifted emissivity minima to ~1100 and 465 cm^{-1}.

mode [*Minitti et al*., 2007]. The feature has been noted to change in depth with viewing angle for natural and synthetic amorphous silica [*Almeida*, 1992; *Ruff et al*., 2011]. The feature can also be completely absent from spectra of surfaces that otherwise look like silica-rich coatings/leached rinds—for example, it is not present in the spectrum of ICE170 altered in Acid A, but it is present in the spectrum of BAS101 altered in Acid A (Figure 6). It is unknown what would cause the feature to be absent, but suggestions include the effects of coating thickness [*Crisp et al*., 1990; *Kraft et al*., 2003] and/or material porosity (Ruff, personal communication, 2014).

Crisp et al. [1990] found that all three spectral features associated with silica-rich coatings/layers (~1090–1100, 465, and 1220 cm^{-1} shoulder features) are very common in spectra from lava flows over 50 years old, which presumably have well-developed silica-rich coatings. Flows that are weeks old also have spectral features associated with silica-rich coatings/layers, but the 1220 cm^{-1} shoulder feature is usually absent. Likewise, *Kraft et al*. [2003] measured TIR spectra of Columbia River Basalt coated with varying thicknesses of amorphous silica and found that the 1220 cm^{-1} spectral feature did not appear until the coatings were ~3 μm thick. These studies suggest that the feature only becomes present when the silica-rich coating/layer is of sufficient thickness. However, *Minitti et al*. [2007] found that one sample with silica-rich coatings/layers ~2–3 μm thick (MUO) had the 1220 cm^{-1} spectral shoulder, while another sample with generally thicker coatings/layers (~5–7 μm; MIY) did not. Thus, there must be other factors controlling the presence or absence of the 1220 cm^{-1} shoulder feature.

We hypothesize that the presence or absence of the 1220 cm^{-1} spectral feature is due to the overall percentage of silica making up the outer surface of the sample. The 1220 cm^{-1} feature is present in the spectra of basalt glass altered in Acid A, but not in the spectra of the more crystalline basalt altered in Acid A. Based on SEM analyses, our companion study found that the basalt glass samples have silica-rich alteration layers that are ~10–100 μm thick, and so the surface measured in the thermal infrared is almost 100% silica-rich material. On the other hand, alteration penetrated the interior of the glassy basalt sand grain samples (ICE170), leaving parts of the surface of the grains relatively unaltered, so that the fraction of silica-rich material measured in the thermal infrared was much less. The silica-rich phases in both the basalt glass and the glassy basalt were fractured and porous, so we do not think porosity is causing the spectral difference in this case [*Smith et al*., 2017].

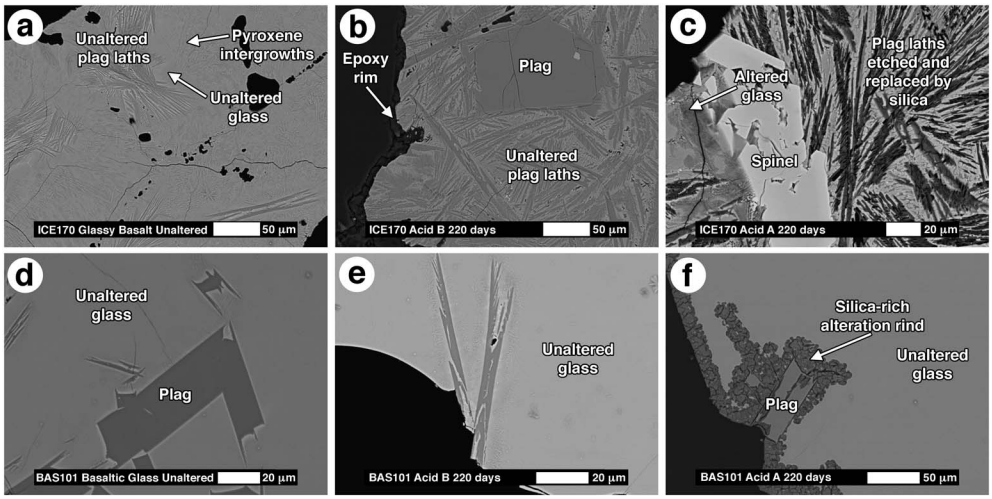

Figure 15. Scanning electron microscope (SEM) images of cross sections of glassy basalt (ICE170) and basaltic glass (BAS101) sand grains before and after 213 days of alteration in Acid B (starting pH ~ 3) and Acid A (starting pH ~ 1). White bars indicate scale for each image. (a) Unaltered ICE170, showing plagioclase feldspar crystals (laths) surrounded by a glassy matrix and significant interior fractures. (b) ICE170 grain after alteration in Acid B, showing no obvious alteration features (note that the dark rim corresponds to epoxy used to secure grains in place). (c) ICE170 grain after alteration in Acid A, showing pervasive etching, leaching of glass, and replacement of plagioclase by silica. (d) Unaltered BAS101, showing homogeneous glass with minimal fracturing. (e) BAS101 grain after alteration in Acid B, showing no obvious signs of alteration. (f) BAS101 grain after alteration in Acid A, showing ~20 μm thick silica-rich and porous rind on outer surfaces and along near-surface fractures only.

5.4. Effects of Surface Texture on Thermal IR Spectra

The detailed thermal infrared analysis presented above is limited to the sand-sized samples, as thermal infrared spectra were acquired after the completion of the experiment, and we were only able to save grains from each stage of the experiment. This level of analysis was not possible for the large centimeter-scale fragment samples. However, we can draw some conclusions about the effects of weathering on the surfaces of the centimeter-scale fragments based on the spectra of the final altered samples, as shown in Figure 14. Fragment samples of BSB101 are not shown, as this sample was collected in the field as sand.

After 213 days of alteration, naturally rough surfaces of the fragments (black lines in Figure 14) are spectrally similar to the equivalent sand grain spectra (blue lines in Figure 14), suggesting that our interpretations of weathering processes hold for granular sediments as well as most rocks. However, the artificially smooth cut surfaces (gray lines in Figure 14) consistently exhibit silica absorption bands near 1100 and 465 cm^{-1} in all experiments except BAS101. In the Acid A (pH ~ 1) experiments, these bands are deeper than those in the equivalent sand or natural surface spectra. On the glass sample (BAS101), the somewhat stronger silica bands appear to correlate with strong linear blue slopes in the near infrared, consistent with a depositional silica coating. In the Acid B experiments (pH ~ 3), silica bands are present in the thermal infrared spectra of the cut surfaces of the basalts, even though no silica bands are detected in any of the near-infrared spectra of these samples. For the glass (BAS101), silica bands are present in spectra of the natural surface and are correlated with a strong concave-up blue slope in the near infrared on the unaltered samples, suggesting that the natural surface of this sample has a preexisting leached rind that was not affected by the pH 3 solution. While the strong silica bands in the basalts would also seem to imply an additive effect like in a coating, this is not consistent with near-infrared results for those samples. Thus, the form of the silica indicated by thermal infrared spectra on the cut surfaces of the basalts is unclear.

6. Microscopic Properties From SEM

Detailed SEM results are discussed in our companion paper [*Smith et al.*, 2017] but are summarized briefly here. Key SEM images are shown in Figure 15. SEM observations of starting materials indicate that the key physical differences between BAS205, ICE170, and BAS101 are crystallinity and fracture length. BAS205

contains diverse phenocrysts of plagioclase, pyroxene, and olivine, with no clear concentrations of glass, and abundant fractures hundreds of microns long that extend away from the rim of the grain. ICE170 is less crystalline than BAS205 with large areas of glassy matrix but exhibits many radiating plagioclase crystals and some isolated pyroxene crystals, as shown in Figure 15a. ICE170 also exhibits numerous long fractures, similar to BAS205. In contrast, BAS101 is much more homogeneous and glassy, containing only isolated plagioclase crystals, and only very short fractures (tens of microns in length that run parallel to grain boundaries, as shown in Figure 15d). BSB101 starting materials looks very similar to BAS101.

Upon alteration for 213 days in Acid B (starting pH ~ 3), none of our samples show clear evidence for alteration in SEM imagery, either surface alteration in the form of rinds and coatings or alteration in the interior of the grains (Figures 15b and 15e). The only evidence for alteration comes from SE images of ICE170 grain surfaces, which exhibit micrometer-scale etch pits and pit chains with collapse-like internal morphologies suggestive of a dissolution process. BAS101 does not exhibit any obvious dissolution features in SE images of grain surfaces.

Alteration for 213 days in Acid A (starting pH ~ 1) has much clearer effects on all samples in SEM. BAS205 and ICE170 show evidence for pervasive alteration throughout the samples, including dissolution of plagioclase and replacement by silica (dark laths in Figure 15c), as well as leaching of glass to form silica-enriched regions. Where these altered regions intersect the surface of the grain, they display a highly fractured texture in SE images. In contrast, alteration of the BAS101 and BSB101 glasses is entirely restricted to the surface of the samples, where a silica-rich, fractured, and continuous alteration rind several micrometer to tens of micrometer thick is present (Figure 15f). In SE images, this rind has a surface texture varying from honeycomb-like to highly fractured.

7. Weathering Under Moderately Acidic Conditions

Our spectral observations and interpretations are summarized in Table 4. Both visible/near-infrared and thermal infrared observations indicate that weathering at moderate pH (Acid B, starting pH ~ 3) for 213 days on naturally textured surfaces results in no clear spectral signatures of surface alteration for crystalline basalt, and only very subtle signatures of alteration for most of the glassy samples, and did not modify preexisting silica-rich coatings on one glassy sample (BAS101 natural surface). Even for the glassy samples, these subtle signatures are only detectable in the thermal infrared spectra, which show a clear enrichment in mafic phases (mainly glass and olivine if present). In all cases in the near infrared, the spectra after 200 days of alteration are almost indistinguishable from their unaltered counterparts, with only minor changes in the strengths of some mafic bands and subtle changes in spectral slopes occurring in some samples. Thermal infrared spectra also generally show no added alteration phases. The lack of alteration rinds suggests that some dissolved phases like silica remained in solution and thus were removed from the system when the fluids were refreshed. Other dissolved phases may have also been deposited as easily soluble and surficial secondary phases that were removed upon rinsing of the sample. In support of this observation, SEM results show no alteration phases or coatings adhered to the samples in the Acid B (starting pH ~ 3) experiments [*Smith et al.*, 2017]. The only exception was our observation of minor silica in thermal IR spectra (but not near-IR spectra) of BAS205, which, with time, could possibly develop into a more prominent alteration coating or other alteration phase. The precipitation of silica in BAS205 and not the other samples may be due to greater abundance of olivine in this sample, as observed in previous acid alteration studies [e.g., *Tosca et al.*, 2004; *Golden et al.*, 2005; *Hurowitz et al.*, 2005].

However, thermal infrared spectra of natural surfaces do consistently show two subtle spectral changes that we attribute to alteration, which may also help to explain the even more subtle changes in near-infrared spectra: (1) some loss of mafic minerals, presumably due to preferential dissolution and (2) a shift of Si–O glass absorption to wavelengths lower than expected for basaltic glass, perhaps due to depolymerization.

7.1. Preferential Dissolution of Primary Minerals

In a simple model of basalt dissolution, minerals with higher solubilities should dissolve first. Both plagioclase and glass exhibit solubilities that are dependent on pH, but at the starting pH of Acid B (~3), pyroxene and plagioclase should have comparable solubilities, and glass exhibits a solubility higher than these phases

Table 4. Summary of Spectral Interpretations

	Near Infrared	Thermal Infrared	Modeled Glass (wt %)	Alteration Mechanism
		Starting Mineralogy in Order of Decreasing Abundance (Inferred or Modeled)		
BAS205	Olivine, HCP, Plagioclase	Plagioclase, Glass, Oxides, Olivine, HCP	17	
ICE170	HCP, Olivine, Glass	Glass, HCP, Olivine, minor Plagioclase	50	
BAS101	Glass	Glass, minor CPX, minor Oxide	77	
BSB101	Glass, Olivine	Glass, Olivine	86	
		Acid A: Effects of Alteration (Starting pH ~ 1)		
BAS205	Addition of minor hydrated silica Relative increase in pyroxene Loss of oxides	Increased silica and sulfates Increased polymerization Relative increase in plagioclase/pyroxene due to loss of glass/oxides		Acid infiltrates sample interior, where crystals are dissolved and replaced with poorly crystalline silica phases
ICE170	Hydrated silica coating Relative increase in pyroxene due to loss of glass/olivine Loss of oxides	Increased silica Increased polymerization Relative increase in pyroxene due to loss of glass/olivine/plagioclase		
BAS101	Leached rind on glass Hydrated silica coating Loss of oxides	Complete replacement by high-silica phases		Acid infiltrates near the surface of glass and causes local dissolution and reprecipitation to form a silica-rich leached rind
BSB101	Leached rind on glass Hydrated silica coating Loss of olivine Loss of oxides	Complete replacement by high-silica phases		
		Acid B: Effects of Alteration (Starting pH ~ 3)		
BAS205	No effect	Addition of minor silica Loss of glass and oxides		Minimal alteration via stoichiometric dissolution of all phases
ICE170	Relative increase in olivine due to loss of pyroxene	Relative increase in glass/olivine due to loss of pyroxene and plagioclase Decreased polymerization		Preferential dissolution of fine-grained mafics relative to coarser grains and glass, as well as surficial depolymerization of glass
BAS101	Addition of iron oxides Addition of iron oxides	Loss of all phases other than mafic glass Decreased polymerization		
BSB101	Addition of iron oxides	Relative loss of olivine Decreased polymerization		

but lower than olivine [*Hausrath et al.*, 2008]. Thus, olivine should dissolve the fastest, followed by glass and then pyroxene and plagioclase at similar rates. This simple model generally works when applied to our crystalline basalt (BAS205), which experiences some loss of mafic phases (mainly glass) relative to plagioclase when altered by either moderately or highly acidic solutions. However, this simple solubility model is not consistent with our observation of a loss of pyroxenes relative to glass in the glassy sample BAS101 after alteration at pH ~ 3.

We hypothesize that preferential dissolution of pyroxene in BAS101 at pH ~ 3 is most likely driven by crystal grain size. Finer crystals have higher surface area to volume ratios than do large crystals and thus dissolve more quickly. In SEM images of BAS205 presented in the companion paper to this study [*Smith et al.*, 2017], plagioclase, olivine, and pyroxene are all easily identified as large crystals of similar sizes. In contrast, BAS101 and BSB101 tend to exhibit only large plagioclase crystals, surrounded by a glassy matrix. Thus, the pyroxene identified in both near-IR and TIR spectra must be present in the glassy matrix, perhaps as devitrified glass. These small crystals would be much more susceptible to dissolution than if they were present as larger grains. In support of this hypothesis, we also observe the loss of pyroxene relative to olivine in ICE170,

and only the olivine is present as larger grains in SEM images of this sample. However, under highly acidic alteration (pH ~ 1), ICE170 does exhibit loss of glass/olivine relative to pyroxene (Table 4), perhaps suggesting that solubility dominates over grain size effects at lower pH.

7.2. Depolymerization of Basaltic Glass

The other spectral change that we observe in thermal infrared spectra of glassy samples weathered under moderately acidic conditions is a shift of Si–O glass absorption to wavelengths lower than expected for basaltic glass. This effect is most notable in BAS101, which shifts from ~1010 cm^{-1}, typical for basaltic glass, to ~970 cm^{-1}. In BSB101, the shift is similar but less strong, from ~980 to ~960 cm^{-1}. This change is modeled as a significant increase in the proportion of basaltic glass; however, the modeled fit is unable to replicate the low band minimum of the spectrum, suggesting that basaltic glass alone is insufficient to explain the spectral changes. Instead, this shift could also be caused by decreased polymerization in the sample surface.

Silicate glass is composed of SiO_4 tetrahedra linked by shared (bridging) oxygens. The degree of polymerization of a glass or mineral refers to how well interlinked the tetrahedra are, as measured by the number of bridging oxygens. A silicate becomes less polymerized or depolymerized when those oxygens are bonded to cations other than Si^{4+}. This can occur due to the presence of other cations like Na^{+}, Ca^{2+}, Mg^{2+}, $Fe^{2+/3+}$, or Al^{3+}, none of which are capable of bonding with as many oxygens as Si^{4+}, or due to the presence of water, which reacts with bridging oxygen to form hydroxyl molecules. Thus, the more mafic a glass or mineral is, the less polymerized it is. The end-members of this trend are quartz, which can be totally polymerized, and olivine, which is totally depolymerized. Hydrated silica and opal are slightly less polymerized than quartz because they often contain Al substituted for Si. The apparent depolymerization of the mafic glasses during moderately acidic leaching may thus be due to a relative increase in mafic network-modifying cations, a decrease in their oxidation state (e.g., Fe^{3+} either reduced to or preferentially removed over Fe^{2+}), or the addition of water.

The more crystalline ICE170 glassy basalt also exhibits increased absorption near ~940 cm^{-1} after weathering at moderately acidic pH. Given the partially glassy nature of this sample, we hypothesize that this shift is due to a combination of increased exposure of olivine and mafic glass at the expense of other phases and to decreasing polymerization in the glass.

The process and spectral effects of depolymerization are both distinct from those of devitrification, which is a partial recrystallization of glass that occurs when it is maintained at high temperatures after quenching. During devitrification, disordered glass structures form more ordered chains and sheets that can eventually lead to crystallization of mineral phases like pyroxene [e.g., *Cook et al*., 1990]. Devitrified glass has a distinct thermal infrared signature, where the initial symmetrical U-shaped glass band centered near 990 cm^{-1} splits into an asymmetrical doublet with centers near 1050 and 900 cm^{-1}, corresponding to the sheets and chains, respectively [*Crisp et al*., 1990; *Farrand et al*., 2016]. These band positions and shapes are distinctly different from the much smaller shift we observe in glass on exposure to moderately acidic solutions, which is from ~1010 initially to ~970 cm^{-1} after exposure. This suggests that we are not observing a structural reordering like devitrification and that the process may be due to a bulk process like leaching or addition of specific elements, as discussed above. Lastly, one consequence of the significant spectral difference between the various acid-leached glasses presented here and the devitrified glasses presented by *Farrand et al*. [2016] is that we should be able to uniquely identify and differentiate these two types of glass modification/alteration in planetary surface spectra.

Depolymerization may be affecting the near-infrared spectra of the glasses as well. All three partially to fully glassy samples altered at moderately acidic pH also exhibit red slopes in the near infrared. Previously, red slopes in glasses have been associated with greater reduced or metallic iron content [*Moroz et al*., 2009], which suggests that the red slopes that we observe could be consistent with depolymerization due to a relative increase in reduced iron. While we can neither confirm nor refute this hypothesis based on our results, the red slopes do appear to be correlated with spectral evidence for depolymerization in the midinfrared.

8. Weathering Under Highly Acidic Conditions

In contrast to the moderate-pH experiments, both visible/near-infrared and thermal infrared observations indicate that weathering at low pH (Acid A, starting pH ~ 1) for 213 days results in clear spectral signatures

of alteration. In the visible/near infrared, most samples develop clear absorption bands near 2.21 μm and sometimes 1.9 μm, and in glassy samples, these bands are superposed on strong concave-up blue spectral slopes. Thermal infrared spectra of all samples show the development of absorption bands near 1090 and 465 cm^{-1}. These spectral changes could all be attributed to silica in some form. A key constraint on the nature of the silica is that the silica spectral signatures persist after repeated rinsing of the samples, suggesting that they are due to a depositional coating, a leached rind, or pervasive alteration of the sample. However, the mode and extent of alteration appear to vary between the samples, as indicated by variations in the strength of VNIR spectral slopes, VNIR absorption bands, and TIR absorption bands. Indeed, all of these spectral features generally appear to increase in strength along with the fraction of glass in the samples.

8.1. Effects of Crystallinity on Mode of Alteration

Based on visible/near-infrared and thermal infrared spectral analysis along with SEM observations, degree of crystallinity appears to determine the type of surface alteration that basalts experience. The crystalline sample (BAS205) showed only weak spectral signatures of hydrated silica in both the visible/near infrared and thermal infrared, while the partly glass basalt (ICE170) showed clear addition of hydrated silica, and the fully glassy basalt and basaltic sand (BAS101 and BSB101) both became spectrally dominated by silica (with variable hydration). Furthermore, visible/near-infrared spectral slopes consistent with leached rinds or coatings were only observed on the fully glassy samples.

SEM observations of altered samples in our companion paper confirm that there are significant physical differences between partially glassy and fully glassy samples [*Smith et al*., 2017]. Of the samples examined using SEM, only the fully glassy sample (BAS101) showed clear evidence for the development of silica-enriched rinds or coatings on the exterior of the sample. While our SEM compositional profiles do not have sufficient resolution to uniquely differentiate a silica-rich replacement layer from a true leaching rind with a very sharp compositional boundary, the layers are 10–100 μm thick—often much thicker than expected for a leached layer (1–10 μm) [e.g., *Chemtob et al*., 2010]. Thus, we hypothesize that the external alteration took place via localized dissolution and reprecipitation to form a leached rind.

In contrast, the partially glassy sample (ICE170) does not show evidence for an exterior rind or coating and instead shows evidence for pervasive alteration penetrating into the interior of the sample. The interior of the sample is characterized by a relatively unaltered glassy matrix surrounding silica-rich zones that appear to have replaced plagioclase quench crystals. Indeed, the presence of crystals appears to control the movement of alteration fluids within the sample, as alteration zones tend to propagate along crystal boundaries.

These SEM observations suggest that alteration is restricted to the surface for glass but rapidly penetrates into the interior of even partially crystalline samples, due to the fluid pathways enabled by fractures and crystal boundaries. Because spectral investigations are only sensitive to the upper few microns of the surface, the glass exhibits stronger signatures of alteration than the less glassy sample, even though the latter is much more pervasively altered. We assume that these results extend to highly crystalline samples as well. SEM analysis was only performed on unaltered BAS205, but given that these images showed long fractures penetrating the unaltered sample to depth and that BAS205 showed minimal evidence for surface alteration in either VNIR or TIR spectra, we hypothesize that any alteration that occurred was also dominantly in the interior of BAS205.

8.2. Comparison to Natural Silicic Coatings and Rinds

Figure 16 shows spectra of a selection of basalts weathered by hydrothermal vapors/fluids and sulfuric acid precipitation from Iceland and Hawaii. The samples fall into two clear categories—samples with consistent absorption bands near 0.9, 1.9, and 2.2 μm and variable spectral slopes shown in Figure 16a and samples with consistent blue concave-up spectral slopes and variably present absorption bands at 0.9, 1.9, and 2.2 μm shown in Figure 17b. The samples differ primarily in their crystallinity, as the samples in Figure 16a are fairly typical basaltic lavas, and the samples in Figure 17b are pahoehoe basalt that all exhibit homogeneous glassy cooling rinds [*Chemtob and Rossman*, 2014]. The physical appearance of the two sample sets is also different, as shown in Figure 17, as the samples in Figure 16a appear bright, rough, and orange, yellow, or white in color, while the samples in Figure 16b appear smooth, glossy, and blue, white, yellow, or orange in color.

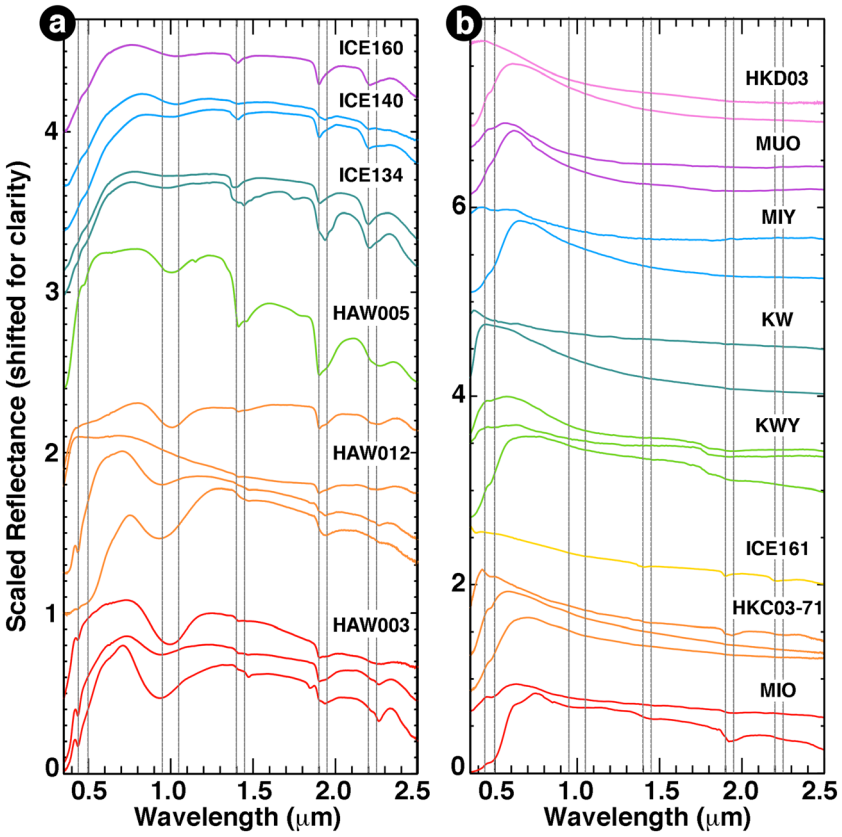

Figure 16. Spectra of naturally altered samples. Color groups correspond to spectra from different parts of the surface of one sample, and vertical lines are positioned at 0.45, 0.50, 0.95, 1.05, 1.40, 1.45, 1.90, 1.95, 2.20, and 2.25 μm. (a) Siliceous and sulfurous coatings, exhibiting silica bands near 1.90 and 2.20 μm and Fe sulfate bands near 0.95, 1.95, and 2.26 μm. (b) Leached glasses, exhibiting blue concave-up spectral slopes and, sometimes, 1.9 and 2.2 μm silica bands. HAW003, HAW012, and HAW005 are coated basalts from Kilauea Caldera, Hawaii; ICE134, ICE140, ICE160, and ICE161 are weathered basalts from hydrothermal vents in Hveragerði, Iceland. HKD03, HKC03-71, MIY, MIO, MUO, KW, and KWY are leached pahoehoe basalts with glassy cooling rinds from the Ka'u Desert, Kilauea, Hawaii [*Minitti et al.*, 2007; *Seelos et al.*, 2010].

This variability in color often appears on a given sample and is reflected in the significant spectral variability of these surfaces shown in Figure 16.

We interpret the spectra in Figure 16a as consistent with a variable mixture of hydrated or opaline silica (indicated by absorption bands at 1.4, 1.9, and 2.2 μm, sometimes with a strong shoulder at 2.25 μm) and ferric sulfates like jarosite (indicated by absorption bands at 0.44, 0.95, 1.48, 1.95, and 2.26 μm). The silica absorption bands in the sulfate-free spectra in this group resemble the silica bands in our more crystalline samples weathered under strongly acidic conditions, although the spectral signature of the underlying basalt is completely masked in the natural samples. Although we see more evidence for volumetric alteration rather than physical coating development in our more crystalline samples, we suggest either these samples could develop thick coatings after exposure to a more closed system than our simulation provided or that long enough exposure would cause the surface of the sample to become fully altered to silica at depth, which would resemble a coating physically and spectrally.

We interpret the spectra in Figure 16b as consistent with leached rinds on glass (as indicated by the strong concave-up blue spectral slope) with additional precipitated silica (as indicated by absorption bands at 1.4, 1.9, and 2.2 μm) and Fe/Ti oxide coatings (as indicated by absorption bands near 0.5 μm and overall decreased reflectance shortward of 0.6 μm). These spectra are quite similar to spectra of glass samples altered under strongly acidic conditions, confirming previous results that these rinds are formed in open hydrologic systems where limited deposition from solution occurs [*Minitti et al.*, 2007; *Chemtob et al.*, 2010; *Chemtob and Rossman*, 2014]. In addition, although both sets of samples shown in Figures 16 and 17 exhibit evidence for

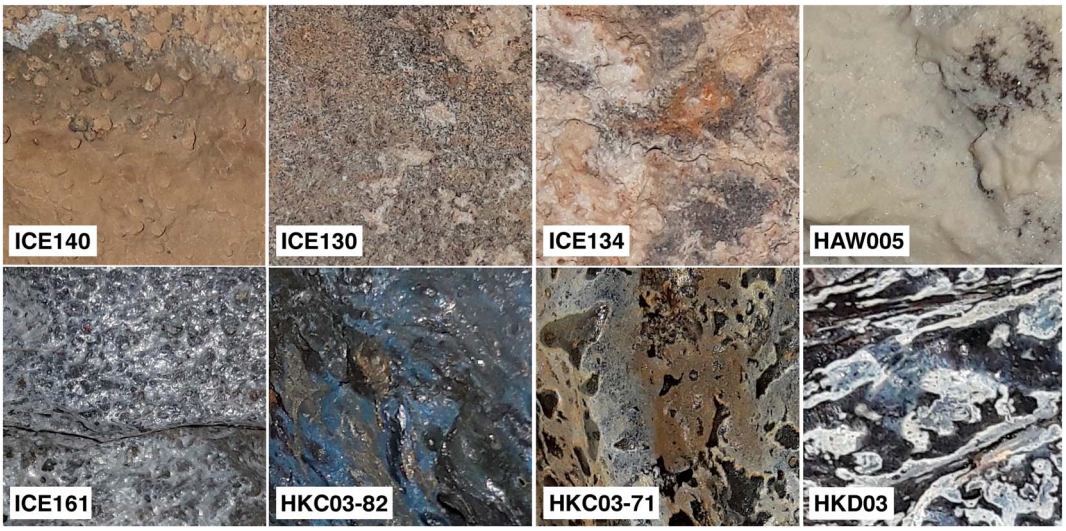

Figure 17. Photos of naturally weathered and coated basalt surfaces, corresponding to a subset of spectra shown in Figure 16. The top row shows siliceous and sulfurous coatings on basalt, and the bottom row shows leached rinds and coatings on glass. All images are approximately 2 cm wide.

some type of silica coating, silica coatings on basalt and silica coatings/rinds on glass are quite spectrally distinct, supporting this same result from our laboratory leaching study.

9. Implications for Mars

The results of this study show that the spectral signatures of acid alteration should persist in mafic sediments or surface bedrock units on Mars even when sulfates and other secondary alteration products have been removed by subsequent aqueous activity or physical abrasion. However, the visible/near-infrared and thermal infrared spectral signatures of acid alteration vary depending on the acidity of the solution, and this has major implications for our interpretation of the alteration history of the Martian surface.

9.1. Detecting Moderately Acidic Alteration in Spectral Data Sets

One of the most surprising results of this study is that moderately acidic solutions do not cause major compositional changes to basalts or glasses undergoing alteration. Indeed, this type of alteration in an open system produces no obvious evidence of coatings, rinds, or other physical alteration phenomena in the visible/near infrared, with the exception of a red spectral slope that would be difficult to differentiate from typical Martian dust. However, the thermal infrared appears to be more sensitive to alteration of basalts and glassy basalts by these moderately acidic solutions (e.g., pH ~ 3). Together, a combination of anomalously low Si–O band minima (e.g., below 1000 cm^{-1}) and high pyroxene/glass, pyroxene/olivine, or plagioclase/pyroxene ratio in thermal infrared spectra could indicate this type of moderately acidic weathering. However, detecting these weak spectral effects in a planetary data set in the absence of secondary weathering products may be challenging. Thus, in an open hydrologic system exposed to multiple aqueous events or to postdiagenesis physical modification that removes friable secondary alteration products, moderately acidic weathering might leave no clear spectral signature on the weathered parent material.

9.2. Detecting Strongly Acidic Alteration in Spectral Data Sets

Both visible/near-infrared and thermal infrared spectral data sets should be able to detect residual silica coatings and dissolution/replacement zones caused by alteration in strongly acidic solutions (e.g., pH ~ 1), even when other secondary products have been removed from the system. Both spectral ranges are sensitive to silica deposited during strong acid leaching, and thus, ideally, both data sets should detect hydrated silica absorption bands in most locations where significant acid leaching has occurred. Visible/near-infrared spectra can also indicate the presence of coatings/leached rinds that appear to uniquely form on glass during strongly acidic alteration. Natural surfaces of altered glasses exhibit strong concave-up blue spectral slopes in the visible/near infrared, and in the thermal infrared, these slopes appear to be correlated with a strong

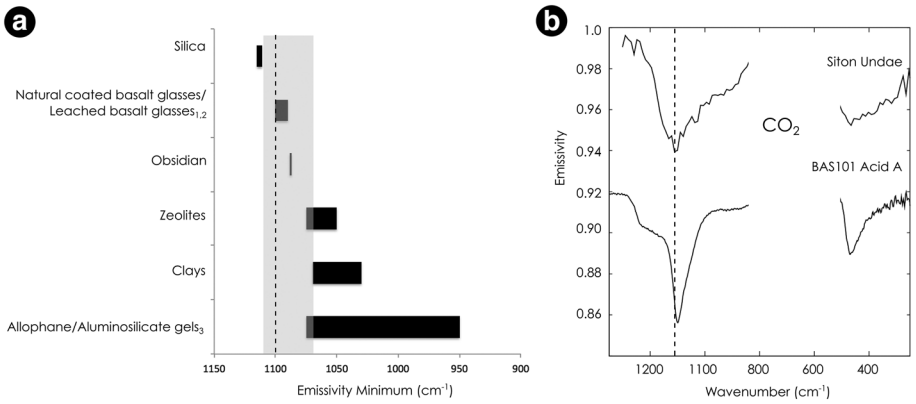

Figure 18. (a) Plot comparing the TIR Si–O stretching emissivity minima ranges of some "high-silica" phases. All data were taken from *Michalski et al.* [2005] except (1) *Minitti et al.* [2007], (2) *Horgan et al.* [this study], and (3) *Rampe et al.* [2012]. The gray box indicates the range of emissivity minima for TES Surface Type 2 spectra between 1070 and 1110 cm^{-1} [*Michalski et al.*, 2005], and the dashed line marks the emissivity minimum position of TES spectra from Siton Undae shown in Figure 18b. (b) Average TIR spectrum from Siton Undae (centered at 293.80°E, 74.80°N) compared to the spectrum of BAS101 grain samples exposed to Acid A for 213 days. Dashed line is in same position as in Figure 18a.

1200 cm^{-1} shoulder on the 1100 cm^{-1} silica absorption band, which we interpret as indicating high abundances of amorphous silica. This is even though visible/near-infrared hydrated silica bands are generally not present in spectra of leached surfaces that exhibit the strongest spectral slopes due to rinds (Figure 2) [*Minitti et al.*, 2007]. Thus, thermal infrared silica detections correlated with visible/near-infrared concave slopes could also be a good indicator of past strongly acidic alteration.

It is important to note that the experiments in this study were conducted at room temperature but that mineral solubilities and other important parameters that control the kinetics and mode of alteration are strongly dependent on environmental variables like fluid temperature. Thus, the spectral signatures discussed here are indicative of stronger or weaker acid solutions and, if detected on Mars, should not be interpreted as indicating a specific pH range.

9.3. Implications for TES Surface Type 2

Globally, TES Surface Type 2 is somewhat variable and displays a range of spectral shapes. This is demonstrated in Figure 18 by the large range of Si–O band emissivity minima that Surface Type 2 areas exhibit (1075–1110 cm^{-1}) [*Michalski et al.*, 2005]. While this range encompasses the emissivity minima exhibited by basalt and basaltic glass altered at low pH in our experiments (~1090–1100 cm^{-1}), it is also consistent with a variety of other high-silica phases. However, the range of acceptable minima shrinks considerably if we consider only the northern plains of Mars (Acidalia Planitia, Utopia Planitia, and the North Polar Sand Sea), where the strongest Surface Type 2 signatures are found. Strong Surface Type 2 signatures in these regions tend to exhibit emissivity minima between 1090 and 1110 cm^{-1} and are best fit using an obsidian end-member with a minimum at ~1087 cm^{-1}. Thus, TES spectra of this type locality for Surface Type 2 are potentially consistent with an acid-altered basalt or basaltic glass in the thermal infrared (Figure 18).

This interpretation of an acid-leached basalt or basaltic glass for the high-silica component of TES Surface Type 2 in the northern plains is supported by the visible/near-infrared spectral shape of the northern plains. As shown in Figure 19b, these areas exhibit a strong concave-up or linear blue slope [*Horgan and Bell*, 2012], similar to the basaltic glass weathered by strongly acidic solutions (pH ~ 1) in our experiments. Indeed, Figure 19a shows that some areas of the North Polar Sand Sea also exhibit broad shallow absorption bands superposed on this concave-up slope that are consistent with an iron-bearing glass like those used in this study [*Horgan and Bell*, 2012].

The combination of both thermal infrared spectral models requiring a high-silica phase and visible/near-infrared spectra consistent with silica-enriched rinds on glass in the northern plains strongly suggests that these regions are at least partially covered in glass-rich materials that have undergone acidic alteration at very low pH. We propose that fluids derived from snow or ice melt at low water:rock ratios are capable of obtaining the acidity needed to form alteration layers on basaltic glass [*Horgan and Bell*, 2012].

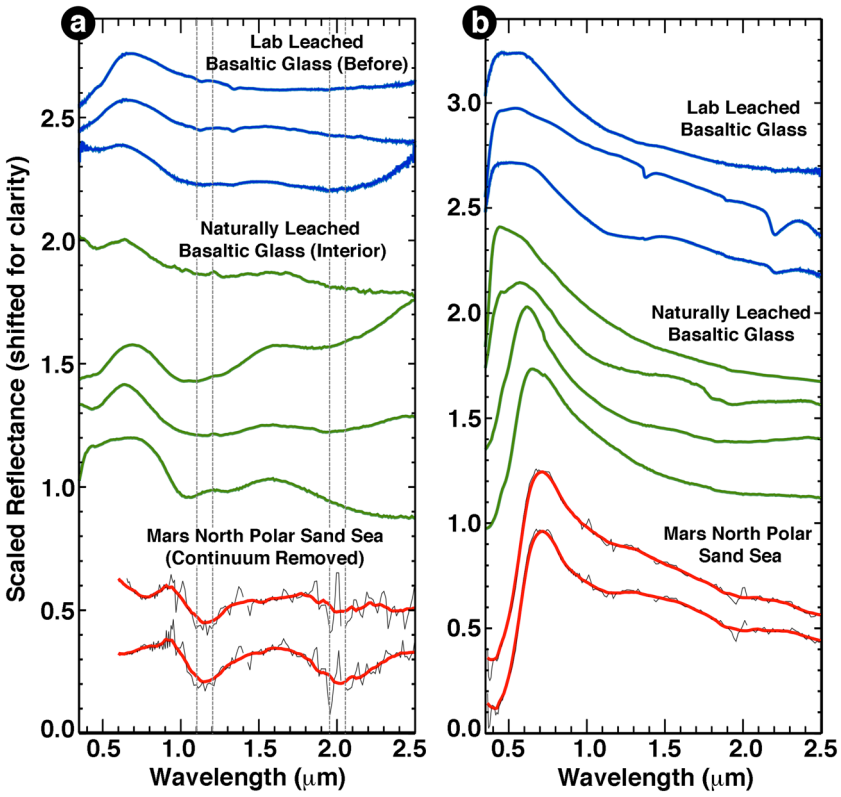

Figure 19. Comparison between OMEGA spectra from the North Polar Sand Sea on Mars interpreted as leached glass (red) [*Horgan and Bell*, 2012], naturally leached glasses (green) [*Minitti et al.*, 2007], and laboratory-leached glasses (blue; BAS101 Acid A). (a) Unaltered glass spectral signatures showing broad iron absorptions near 1.15 and 2 μm. Spectra were acquired from sample surfaces prior to alteration for the laboratory-leached glasses and from the interior beneath the alteration rinds for the naturally leached glasses. OMEGA spectra shown for the Mars North Polar Sand Sea have been ratioed to a dusty spectrum and continuum removed to reveal glass absorption bands compared to the original albedo spectra as shown in Figure 19b. The thick red lines have been smoothed compared to the original spectra, shown as thin gray lines. Dashed vertical lines indicate the ranges over which broad glass absorption bands are typically centered. (b) The altered surfaces of the glass samples in Figure 19a, showing the concave-up spectral shape that we interpret as due to leached rinds on glass.

9.4. Stability of Glass Under Acidic Alteration

Lastly, this study confirms the important but often overlooked fact that glass is actually more stable under long-term acidic alteration than other mafic phases. As discussed above, previous studies have shown that glass has high stability in lower-pH solutions, and our results show that this is due to the fact that glass undergoes dissolution and alteration in a fundamentally different manner than more crystalline samples. SEM analysis of glass and partially crystalline samples show that alteration is restricted to the surface of glasses but penetrates in the interior of more crystalline samples [*Smith et al.*, 2017], likely leading to more pervasive dissolution and alteration of crystalline samples over the long term. This suggests that glass would be more stable than other mafic phases in a dominantly acidic planetary environment. This finding is contrary to the common assumption in studies of Mars that because glass is unstable to weathering at neutral to alkaline pH, the presence of glass at a site indicates that little to no aqueous activity has taken place at that location. Instead, the presence of glass alone indicates only that prolonged aqueous activity at neutral pH has not occurred. Based on our results and previous experiments, if glass is present along with sulfates or halite or exhibits coatings or leaching rinds, this is a strong indication of potentially prolonged aqueous activity at moderately to strongly acidic pH.

10. Conclusions

By submerging basalt and basaltic glasses in highly acidic solutions for 213 days, we have shown that highly acidic alteration (pH ~ 1 at ~20°C and standard atmospheric pressure) produces abundant residual silica on

both basalt and basaltic glasses, but the nature of the silica and the associated alteration mechanism vary with the crystallinity of the sample undergoing alteration. In glassy samples, the alteration is restricted to the surface of the sample and forms a leached, silica-enriched rind via highly localized dissolution and reprecipitation reactions. In crystalline samples, the alteration penetrates into the interior through fractures and along crystal boundaries and causes dissolution and replacement of both matrix and phenocrysts by poorly crystalline high-silica phases in the interior of the samples. One consequence of the difference in alteration styles between glass and crystalline basalt is that glass is actually more stable than crystalline basalt under highly acidic alteration.

While alteration of both glass and basalt at low pH results in silica absorption bands in visible/near-infrared and thermal infrared spectra, only the leached rind on the glass is associated with strong concave-up slopes in visible/near-infrared spectra. Thus, strong silica rind signatures in both visible/near-infrared and thermal infrared spectra of Mars could indicate highly acidic alteration in the past. Indeed, concave-up slopes in the visible/near infrared and strong silica absorptions in the thermal infrared are observed together across large regions of the Martian surface. These regions were previously classified as the silica-enriched TES Surface Type 2, suggesting that at least portions of this major Martian surface type could be the result of widespread acidic alteration.

In contrast, moderately acidic alteration (pH ~ 3 at ~20°C and standard atmospheric pressure) for 213 days does not appear to produce resistant rinds or coatings on either basalt or basaltic glass. The only residual spectral effects on the parent materials are subtle visible/near-infrared slopes and thermal infrared band shifts that we interpret to be due to surficial depolymerization. However, these spectral effects may be difficult to detect in a complex natural setting. Some units and sediments on Mars that have been exposed to acidic solutions may retain no clear sign of alteration, as secondary alteration products that are produced under these moderately acidic conditions (mainly sulfates) may be easily removed by subsequent aqueous activity or abrasion.

Acknowledgments
We thank the Natural Sciences and Engineering Research Council of Canada, the Canadian Space Agency, the Canada Foundation for Innovation, the Manitoba Research Innovations Fund, and the University of Winnipeg for supporting the establishment and operation of the Planetary Spectrophotometer Facility. We also wish to thank Jessica Stromberg for assisting with the acid dissolution experiments and Stan Mertzman for his analysis of the samples. This work was funded in part by the NASA 2001 Mars Odyssey THEMIS project (Jet Propulsion Laboratory contract #1228404 through Arizona State University) and by the Arizona State University Exploration Postdoctoral Fellowship. All visible and near-infrared spectra presented in this work are available from the University of Winnipeg (http://psf.uwinnipeg.ca), and all thermal infrared spectra are available from the TES spectral library (http://speclib.asu.edu).

References

Adams, J. B. (1968), Lunar and Martian surfaces: petrologic significance of absorption bands in the near-infrared, *Science*, *159*(3), 1453–1455, doi:10.1126/science.159.3822.1453.

Adams, J. B., C. Pieters, and T. B. McCord (1974), Orange glass—evidence for regional deposits of pyroclastic origin on the moon, *Lunar Sci. Conf.*, *5*, 171–186.

Almeida, R. M. (1992), Detection of LO modes in glass by infrared reflection spectroscopy at oblique incidence, *Phys. Rev. B*, *45*(1), 161, doi:10.1103/PhysRevB.45.161.

Atkinson, S. S. (1990), Geochemical and isotopic study of the Roza member feeder system, Columbia River Basalt Group; MSc thesis, University of Alberta, Edmonton, AB, 112 pp.

Bandfield, J. L., V. E. Hamilton, and P. R. Christensen (2000), A global view of Martian surface compositions from MGS-TES, *Science*, *287*, 1626, doi:10.1126/science.287.5458.1626.

Banin, A., F. X. Han, I. Kan, and A. Cicelsky (1997), Acidic volatiles and the Mars soil, *J. Geophys. Res.*, *102*, 13,341, doi:10.1029/97JE01160.

Berger, G., C. Claparols, C. Guy, and V. Daux (1994), Dissolution rate of a basalt glass in silica-rich solutions: implications for long-term alteration, *Geochim. Cosmochim. Acta*, 58, 4875–4886.

Bibring, J.-P., et al. (2006), Global mineralogical and aqueous Mars history derived from OMEGA/Mars Express Data, *Science*, *312*, 400–404, doi:10.1126/science.1122659.

Brown, A. J. (2014), Spectral bluing induced by small particles under the Mie and Rayleigh regimes, *Icarus*, *239*(C), 85–95, doi:10.1016/j.icarus.2014.05.042.

Cheek, L. C., and C. M. Pieters (2014), Reflectance spectroscopy of plagioclase-dominated mineral mixtures: implications for characterizing lunar anorthosites remotely, *Am. Mineral.*, *99*(10), 1871–1892, doi:10.2138/am-2014-4785.

Chemtob, S. M., and G. R. Rossman (2014), Timescales and mechanisms of formation of amorphous silica coatings on fresh basalts at Kīlauea Volcano, Hawai'i, *J. Volcanol. Geoth. Res.*, *286*, 41–54, doi:10.1016/j.jvolgeores.2014.08.029.

Chemtob, S. M., B. L. Jolliff, G. R. Rossman, J. M. Eiler, and R. E. Arvidson (2010), Silica coatings in the Ka'u Desert, Hawaii, a Mars analog terrain: a micromorphological, spectral, chemical, and isotopic study, *J. Geophys. Res.*, *115*, E04001, doi:10.1029/2009JE003473.

Christensen, P. R., et al. (2001), Mars Global Surveyor Thermal Emission Spectrometer experiment: investigation description and surface science results, *J. Geophys. Res.*, *106*, 23,823–23,872, doi:10.1029/2000JE001370.

Clark, R. N., G. A. Swayze, R. Wise, K. E. Livo, T. M. Hoefen, R. F. Kokaly, and S. J. Sutley (2007), USGS Digital Spectral Library splib06a, *U.S. Geol. Surv., Data Seri.*, *231*.

Cloutis, E. A., and M. J. Gaffey (1991), Spectral-compositional variations in the constituent minerals of mafic and ultramafic assemblages and remote sensing implications, *Earth Moon Planets*, *53*, 11–53, doi:10.1007/BF00116217.

Cloutis, E., F. Hawthorne, S. Mertzman, K. Krenn, M. Craig, D. Marcino, M. Methot, J. Strong, J. Mustard, and D. Blaney (2006), Detection and discrimination of sulfate minerals using reflectance spectroscopy, *Icarus*, *184*(1), 121–157, doi:10.1016/j.icarus.2006.04.003.

Cook, G. B., R. F. Cooper, and T. Wu (1990), Chemical diffusion and crystalline nucleation during oxidation of ferrous iron-bearing magnesium aluminosilicate glass, *J. Non Cryst. Solids*, *120*(1–3), 207–222, doi:10.1016/0022-3093(90)90205-Z.

Crisp, J., A. B. Kahle, and E. A. Abbott (1990), Thermal infrared spectral character of Hawaiian basaltic glasses, *J. Geophys. Res.*, *95*, 21,657–21,669, doi:10.1029/JB095iB13p21657.

Crovisier, J. L., J. Honnorez, and J. P. Eberhart (1987), Dissolution of basaltic glass in seawater: mechanism and rate, *Geochim. Cosmochim. Acta*, *51*(1), 2977–2990, doi:10.1016/0016-7037(87)90371-1.
Dorn, R. I. (1998), *Rock Coatings*, pp. 429 , Elsevier, New York.
Farrand, W. H., T. D. Glotch, J. W. Rice Jr., J. A. Hurowitz, and G. A. Swayze (2009), Discovery of jarosite within the Mawrth Vallis region of mars: implications for the geologic history of the region, *Icarus*, *52*, doi:10.1016/j.icarus.2009.07.014.
Farrand, W. H., S. P. Wright, A. D. Rogers, and T. D. Glotch (2016), Basaltic glass formed from hydrovolcanism and impact processes: characterization and clues for detection of mode of origin from VNIR through MWIR reflectance and emission spectroscopy, *Icarus*, *275*, 1–13, doi:10.1016/j.icarus.2016.03.027.
Feely, K. C., and P. R. Christensen (1999), Quantitative compositional analysis using thermal emission spectroscopy: application to igneous and metamorphic rocks, *J. Geophys. Res.*, *104*, 24,195–24,210, doi:10.1029/1999JE001034.
Fischer, E. M., and C. M. Pieters (1993), The continuum slope of Mars—bidirectional reflectance investigations and applications to Olympus Mons, *Icarus*, *102*, 185–202, doi:10.1006/icar.1993.1043.
Geisler, T., A. Janssen, D. Scheiter, T. Stephan, J. Berndt, and A. Putnis (2010), Aqueous corrosion of borosilicate glass under acidic conditions: a new corrosion mechanism, *J. Non Cryst. Solids*, *356*(28–30), 1458–1465, doi:10.1016/j.jnoncrysol.2010.04.033.
Geisler, T., T. Nagel, M. R. Kilburn, A. Janssen, J. P. Icenhower, R. O. C. Fonseca, M. Grange, and A. A. Nemchin (2015), The mechanism of borosilicate glass corrosion revisited, *Geochim. Cosmochim. Acta*, *158*, 112–129, doi:10.1016/j.gca.2015.02.039.
Gislason, S., and E. Oelkers (2003), Mechanism, rates, and consequences of basaltic glass dissolution: II. An experimental study of the dissolution rates of basaltic glass as a function of pH and temperature, *Geochim. Cosmochim. Acta*, *67*(20), 3817–3832, doi:10.1016/S0016-7037(00)00176-5.
Glass, B. (1984), Tektites, *J. Non Cryst. Solids*, *67*, 333–344, doi:10.1016/0022-3093(84)90158-3.
Golden, D. C., D. W. Ming, R. V. Morris, and S. A. Mertzman (2005), Laboratory-simulated acid-sulfate weathering of basaltic materials: implications for formation of sulfates at Meridiani Planum and Gusev crater, Mars, *J. Geophys. Res.*, *110*, E12S07, doi:10.1029/2005JE002451.
Grambow, B. (2006), Nuclear waste glasses-how durable? *Elements*, *2*(6), 357.
Hausrath, E. M., and S. L. Brantley (2010), Basalt and olivine dissolution under cold, salty, and acidic conditions: what can we learn about recent aqueous weathering on Mars? *J. Geophys. Res.*, *115*, E12001, doi:10.1029/2010JE003610.
Hausrath, E. M., A. K. Navarre-Sitchler, P. B. Sak, C. I. Steefel, and S. L. Brantley (2008), Basalt weathering rates on Earth and the duration of liquid water on the plains of Gusev crater, Mars, *Geology*, *36*(1), 67–70, doi:10.1130/G24238A.1.
He, G. S., H.-Y. Qin, and Q. Zheng (2009), Rayleigh, Mie, and Tyndall scatterings of polystyrene microspheres in water: wavelength, size, and angle dependences, *J. Appl. Phys.*, *105*(2), 023,110, doi:10.1063/1.3068473.
Hellmann, R., R. Wirth, D. Daval, J.-P. Barnes, J.-M. Penisson, D. Tisserand, T. Epicier, B. Florin, and R. L. Hervig (2012), Unifying natural and laboratory chemical weathering with interfacial dissolution–reprecipitation: a study based on the nanometer-scale chemistry of fluid–silicate interfaces, *Chem. Geol.*, *294-295*, 203–216, doi:10.1016/j.chemgeo.2011.12.002.
Horgan, B., and J. F. Bell (2012), Widespread weathered glass on the surface of Mars, *Geology*, *40*, 391–394, doi:10.1130/G32755.1.
Horgan, B., E. A. Cloutis, P. Mann, and J. F. Bell (2014), Near-infrared spectra of ferrous mineral mixtures and methods for their identification in planetary surface spectra, *Icarus*, *234*, 132–154, doi:10.1016/j.icarus.2014.02.031.
Hurowitz, J. A., S. M. Mclennan, D. H. Lindsley, and M. A. A. Schoonen (2005), Experimental epithermal alteration of synthetic Los Angeles meteorite: implications for the origin of Martian soils and identification of hydrothermal sites on Mars, *J. Geophys. Res.*, *110*, E07002, doi:10.1029/2004JE002391.
Hurowitz, J. A., N. Tosca, S. Mclennan, and M. Schoonen (2007), Production of hydrogen peroxide in, *Martian Lunar Soils*, *255*(1–2), 41–52, doi:10.1016/j.epsl.2006.12.004.
Hurowitz, J. A., W. W. Fischer, N. J. Tosca, and R. E. Milliken (2010), Origin of acidic surface waters and the evolution of atmospheric chemistry on early Mars, *Nat. Geosci.*, *3*(5), 323–326, doi:10.1038/ngeo831.
Kahle, A. B., A. R. Gillespie, E. A. Abbott, M. J. Abrams, and R. E. Walker (1988), Relative dating of Hawaiian lava flows using multispectral thermal infrared images—a new tool for geologic mapping of young volcanic terranes, *J. Geophys. Res.*, *93*, 15,239–15,251, doi:10.1029/JB093iB12p15239.
King, H. E., O. Plumper, T. Geisler, and A. Putnis (2011), Experimental investigations into the silicification of olivine: implications for the reaction mechanism and acid neutralization, *Am. Mineral.*, *96*(10), 1503–1511, doi:10.2138/am.2011.3779.
Kraft, M. D., J. R. Michalski, and T. G. Sharp (2003), Effects of pure silica coatings on thermal emission spectra of basaltic rocks: considerations for Martian surface mineralogy, *Geophys. Res. Lett.*, *30*(24), 2288, doi:10.1029/2003GL018848.
Kraft, M. D., T. G. Sharp, J. R. Michalski, and E. B. Rampe (2007), Combined thermal and near infrared spectra of hydrous silica coatings: implications for Surface Type 2 mineralogy and recent liquid water on Mars, *38th Lunar Planet. Sci. Conf.*, *38*, 2241.
Langer, K., and O. Florke (1974), Near infrared absorption spectra of opals and the role of water in these SiO_2-nH_20 minerals, *Fortschr. Mineral.*, *52*(1), 17–51.
Lippincott, E. R., A. Van Valkenburg, and C. E. Weir (1958), Infrared studies on polymorphs of silicon dioxide and germanium dioxide, *J. Res. Natl. Bur. Stand.*, *61*(1), 61–70.
Marcucci, E. C., and B. M. Hynek (2014), Laboratory simulations of acid-sulfate weathering under volcanic hydrothermal conditions: implications for early Mars, *J. Geophys. Res. Planets*, *119*, 679–703, doi:10.1002/2013JE004439.
Mcadam, A. C., M. Y. Zolotov, T. G. Sharp, and L. A. Leshin (2008), Preferential low-pH dissolution of pyroxene in plagioclase pyroxene mixtures: implications for Martian surface materials, *Icarus*, *196*, 90–96, doi:10.1016/j.icarus.2008.01.008.
Michalski, J. R., M. D. Kraft, T. G. Sharp, L. B. Williams, and P. R. Christensen (2005), Mineralogical constraints on the high-silica Martian surface component observed by TES, *Icarus*, *174*(1), 161–177, doi:10.1016/j.icarus.2004.10.022.
Michalski, J. R., M. D. Kraft, T. G. Sharp, and P. R. Christensen (2006), Effects of chemical weathering on infrared spectra of Columbia River Basalt and spectral interpretations of Martian alteration, *Earth Planet. Sci. Lett.*, *248*, 822, doi:10.1016/j.epsl.2006.06.034.
Milliken, R. E., et al. (2008), Opaline silica in young deposits on Mars, *Geology*, *36*(1), 847–850, doi:10.1130/G24967A.1.
Minitti, M. E., J. F. Mustard, and M. J. Rutherford (2002), Effects of glass content and oxidation on the spectra of SNC-like basalts: applications to Mars remote sensing, *J. Geophys. Res.*, *107*(E5), 5030, doi:10.1029/2001JE001518.
Minitti, M., C. Weitz, M. Lane, and J. Bishop (2007), Morphology, chemistry, and spectral properties of Hawaiian rock coatings and implications for Mars, *J. Geophys. Res.*, *112*, E05015, doi:10.1029/2006JE002839.
Moroz, L. V., et al. (2009), Spectral properties of simulated impact glasses produced from martian soil analogue JSC Mars-1, *Icarus*, *202*(1), 336–353, doi:10.1016/j.icarus.2009.02.007.

Oelkers, E. H., and S. R. Gislason (2001), The mechanism, rates and consequences of basaltic glass dissolution: I. An experimental study of the dissolution rates of basaltic glass as a function of aqueous Al, Si and oxalic acid concentration at 25°C and pH = 3 and 11, *Geochim. Cosmochim. Acta*, *65*(21), 3671–3681, doi:10.1016/S0016-7037(01)00664-0.

Oguchi, C. (2004), A porosity-related diffusion model of weathering-rind development, *Catena*, *58*(1), 65–75, doi:10.1016/j.catena.2003.12.002.

Petit, J., G. Mea, J. Dran, M. Magonthier, P. Mando, and A. Paccagnella (1990), Hydrated-layer formation during dissolution of complex silicate glasses and minerals, *Geochim. Cosmochim. Acta*, *54*(7), 1941–1955.

Rampe, E. B., M. D. Kraft, T. G. Sharp, D. C. Golden, D. W. Ming, and P. R. Christensen (2012), Allophane detection on Mars with Thermal Emission Spectrometer data and implications for regional-scale chemical weathering processes, *Geology*, *40*(11), 995–998, doi:10.1130/G33215.1.

Ramsey, M. S., and P. R. Christensen (1998), Mineral abundance determination: quantitative deconvolution of thermal emission spectra, *J. Geophys. Res.*, *103*, 577, doi:10.1029/97JB02784.

Rice, M. S., E. A. Cloutis, J. F. Bell, D. L. Bish, B. H. Horgan, S. A. Mertzman, M. A. Craig, R. W. Renaut, B. Gautason, and B. Mountain (2013), Reflectance spectra diversity of silica-rich materials: sensitivity to environment and implications for detections on Mars, *Icarus*, *223*(1), 499–533, doi:10.1016/j.icarus.2012.09.021.

Rogers, A. D., J. L. Bandfield, and P. R. Christensen (2007), Global spectral classification of Martian low-albedo regions with Mars Global Surveyor Thermal Emission Spectrometer (MGS-TES) data, *J. Geophys. Res.*, *112*, E02004, doi:10.1029/2006JE002726.

Ruff, S. W. (1999), Development of Thermal Infrared Emission Spectroscopy for geological investigations of Earth and Mars, *Workshop on Thermal Emission Spectroscopy and Analysis of Dust, Disks, and Regoliths*, abstract 927.

Ruff, S. W., and P. R. Christensen (2007), Basaltic andesite, altered basalt, and a TES-based search for smectite clay minerals on Mars, *Geophys. Res. Lett.*, *34*, L10204, doi:10.1029/2007GL029602.

Ruff, S. W., P. R. Christensen, D. L. Blaney, W. H. Farrand, J. R. Johnson, J. R. Michalski, J. E. Moersch, S. P. Wright, and S. W. Squyres (2006), The rocks of Gusev Crater as viewed by the mini-TES instrument, *J. Geophys. Res.*, *111*, E12S18, doi:10.1029/2006JE002747.

Ruff, S. W., et al. (2011), Characteristics, distribution, origin, and significance of opaline silica observed by the Spirit rover in Gusev crater, Mars, *J. Geophys.Res.*, *116*, E00F23, doi:10.1029/2010JE003767.

Ruiz-Agudo, E., C. V. Putnis, C. Rodriguez-Navarro, and A. Putnis (2012), Mechanism of leached layer formation during chemical weathering of silicate minerals, *Geology*, *40*(10), 947–950, doi:10.1130/G33339.1.

Seelos, K. D., R. E. Arvidson, B. L. Jolliff, S. M. Chemtob, R. V. Morris, D. W. Ming, and G. A. Swayze (2010), Silica in a Mars analog environment: Ka'u Desert, Kilauea Volcano, Hawaii, *J. Geophys. Res.*, *115*, E00D15, doi:10.1029/2009JE003347.

Smith, R. S., B. Horgan, P. Mann, E. A. Cloutis, P. R. Christensen (2017), Acid weathering of basalt and basaltic glass: II. Effects of microscopic alteration textures on spectral properties, *J. Geophys. Res. Planets*, *122*, doi:10.1002/2016JE005112.

Squyres, S., et al. (2004), In situ evidence for an ancient aqueous environment at Meridiani Planum, Mars, *Science*, *306*(5702), 1709–1714.

Techer, I., T. Advocat, J. Lancelot, and J. M. Liotard (2001), Dissolution kinetics of basaltic glasses: control by solution chemistry and protective effect of the alteration film, *Chem. Geol.*, *176*(1–4), 235–263, doi:10.1016/S0009-2541(00)00400-9.

Tosca, N. J., S. M. Mclennan, D. H. Lindsley, and M. A. A. Schoonen (2004), Acid-sulfate weathering of synthetic Martian basalt: the acid fog model revisited, *J. Geophys. Res.*, *109*, E05003, doi:10.1029/2003JE002218.

White, A. F. (1983), Surface chemistry and dissolution kinetics of glassy rocks at 25 C, *Geochim. Cosmochim. Acta*, *47*, 805–815, doi:10.1016/0016-7037(83)90114-X.

White, W. B., and D. G. Minser (1984), Raman spectra and structure of natural glasses, *J. Non Cryst. Solids*, *67*(1–3), 45–59, doi:10.1016/0022-3093(84)90140-6.

Wolff-Boenisch, D., S. R. Gislason, and E. H. Oelkers (2004), The dissolution rates of natural glasses as a function of their composition at pH 4 and 10.6, and temperatures from 25 to 74 C, *Geochim. Cosmochim. Acta*, *68*(23), 4843–4858, doi:10.1016/j.gca.2004.05.027.

Wyatt, M. B., and H. Y. Mcsween (2002), Spectral evidence for weathered basalt as an alternative to andesite in the northern lowlands of Mars, *Nature*, *417*, 263.

Yant, M., A. D. Rogers, H. Nekvasil, Y.-Y. S. Zhao, and T. Bristow (2016), Spectral characterization of acid weathering products on Martian basaltic glass, *J. Geophys. Res. Planets*, *121*, 516–541, doi:10.1002/2015JE004969.

Zent, A. P., and C. P. Mckay (1994), The chemical reactivity of the Martian soil and implications for future missions, *Icarus*, *108*(1), 146–157, doi:10.1006/icar.1994.1047.